Normal Mode Acoustic Scattering Considering Elastic Layers Over a Half Space

by

PAENG, Dong-Guk

B.S., Earth and Marine Sciences, Hanyang University in Korea(1991)
M.S., Earth and Marine Sciences, Hanyang University in Korea(1993)

Submitted to the Department of Ocean Engineering
in partial fulfillment of the requirements for the degree of

Master of Science in Ocean Engineering

at the

MASSACHUSETTS INSTITUTE OF TECHNOLOGY

September 1997

Author .....
Department of Ocean Engineering
August 25, 1997

Certified by .....
Professor Henrik Schmidt
Professor of Ocean Engineering
Thesis Supervisor

Accepted by .....
Professor J. Kim Vandiver
Chairman, Departmental Committee on Graduate Students

Normal Mode Acoustic Scattering Considering Elastic Layers Over a Half Space

by

PAENG, Dong-Guk

Submitted to the Department of Ocean Engineering
on August 25, 1997, in partial fulfillment of the
requirements for the degree of
Master of Science in Ocean Engineering

Abstract

Scattering phenomena due to a rough bottom interface should be studied in order to understand acoustic propagation in shallow water. The normal mode scattering theory and code is developed to compute the scattered field from the rough surface considering elastic layers in the bottom. The extended modal code NMSCAT which was originally developed by Tracey[40] is an efficient approach to calculate scattering in the low frequency and long ranges. The accuracy and validation of the extended NMSCAT code are demonstrated by good agreement within 2 dB error range with the results of the OASS which is based on the wavenumber integral method to be assumed as a reference numerical solution. The elastic-layered bottom is proven to be important to the scattered field in the shallow water waveguide.

The thickness and the properties of one elastic layer affect the scattered field significantly and its effect on scattering is quite different from the effect on the mean field. Parameter studies are performed to analyze the effects on the scattered field. The modal analysis of scattering provides an easy way to understand the scattering phenomena.

The geoacoustic bottom data from an acoustic experiment in the Korea Strait is used to study scattering in emphasis of the effects of two uncertain parameters on the scattered field by the model of the multiple elastic layers. The parameters are the thickness of the first elastic layer and the different elastic properties of the second elastic layer, and the parameters affect the scattered field distinctly in different patterns with the mean field.

Thesis Supervisor: Professor Henrik Schmidt
Title: Professor of Ocean Engineering

Acknowledgments

The fear of the LORD is the beginning of wisdom; all who follow his precepts have good understanding. To him belongs eternal praise. Psalm 111:10
... the mystery of God, namely, Christ, in whom are hidden all the treasures of wisdom and knowledge. Colossians 2:2-3

I would like to thank to my advisor Professor Henrik Schmidt, for your support and encouragement, financially and academically. I cannot express all my gratitude to you with words for your indefatigable patience and deep consideration. I am also grateful to Dr. William Carey for your kindness and willingness. You have provided all the data about the Korea Strait experiment.

I owe a great debt of gratitude to my officemates and Sabina. Sabina has always showed me your kindness and hospitality during two years. Thanks to Dr. Brian Tracey, I can start and finish this work. You are willing to help me in every way all the time. Without Jaiyong Lee, I cannot go forward even one step. I have really enjoyed talking with you over a cup of coffee. I really thank to Vincent Lupien and Kyle Becker who spent their valuable times for proofreading my thesis. Thank you all to my fellow students of the acoustic groups in 5-435.

To my Korean colleagues, Sungeun Kim and Yonghwan Kim, I deeply appreciate you. Both of you always encourage me and take care of me and my wife in every way. I am also grateful to Ohseung Kwon and other church members. I will fondly cherish the memories of the time spent with you to study the Word of God and look forward to a *revival.*

I deeply grateful to my mother and siblings in Korea and father in heaven now. Your sacrifices and love are still the force of my life.

I would like to express special thanks to my wife, Kyoung-Hee Lee. Without you, I cannot spend the hard times even a minute. You always trust me and never complain to be alone even in newly-married days.

Contents

List of Figures

List of Tables

Chapter 1

Introduction

1.1 Motivation

Ocean acoustics is an extremely diverse field with many different types of problems to pursue. One way to categorize ocean acoustics is by the type of ocean to be studied, such as deep water or shallow water acoustics. The different oceans themselves can give some hints to choose the priority of parameters to study and the proper numerical models for research to scientists. After a decade spent studying the deep water phenomena like eddies and global warming, underwater acousticians have turned their interests to shallow water. Following this trend, we will study shallow water acoustics in this thesis.

The characteristics of shallow water are quite different from deep water in terms of propagation of sound in the waveguide. Although deep water has some stochastic phenomena like internal wave and the randomness of medium itself, shallow water is more random because of tides, currents, strong mixing, inhomogeneities of the water itself and the boundaries and so on.

Interactions between boundaries may be one of the most important characteristics in view of sound transmission in shallow water along with volume inhomogeneities like turbulence and solitons[46] as well as sub-bottom inhomogeneities. These complexities challenge sci-

entists to understand scattering in shallow water because scattering becomes important to wave propagation in shallow water.

Many scientists have recently focused on the study of scattering in relation to seafloor characteristics[36][13][37]. In a shallow water waveguide, the acoustic waves interact significantly with the boundaries while they propagate. Especially, the bottom interaction dominates the surface interaction, because shallow water often has a downward refracting sound speed profile. The bottom is often characterized as being rough in shallow water and this roughness brings up the issue of scattering in underwater acoustics. The bottom bounced signals are extremely difficult to analyze due to uncertain knowledge of bottom properties and roughness statistics. However, inverse methods allow bottom properties to be inferred from these complicated bottom interacting signals because the signals contain information about them. Some initial trials have been done to estimate the seafloor parameters by the sound field[9],[25][39, 38, 3]. Here we will study scattering dependent on various parameters of elastic ocean bottoms.

There are many numerical models available to solve acoustic propagation problems but only a few numerical models include scattering. Moreover, most scattering models cannot deal with elasticity in the sub-bottom layers. However, the OASES scattering module OASS, which was developed by Schmidt[31] is based on the wavenumber integral method and considers elastic layers in the bottom. Although this model is very versatile, it requires heavy calculation at long ranges. To compensate for this, Tracey[40] developed a modal theory and code NMSCAT which is more efficient for low frequency and at long ranges than OASS. The modal approach also gives intuitive understanding of the physics of scattering. However Tracey didn't consider arbitrary elastic layers in the sub-bottom structure but elasticity was included only in an elastic half space bottom. In order to study more realistic bottom, effects of the elastic layers on scattering are here included in the numerical model.

The motivation of this thesis is in the development of the theory and numerical code to include arbitrary elastic layers in the sub-bottom structure, based on the modal approach extending the work of Tracey. With this scattering code developed, we will study the effects

of geo-acoustic parameters of layers on scattering in a shallow water waveguide.

1.2 Review of Related Studies

Some recent relevant studies are reviewed in this section along with some numerical models which compute scattering.

Ellis[11] developed a phenomenological normal mode reverberation model which is based on empirical scattering functions. While the normal mode model can provide a good solution to the reverberation problem in shallow water, two major difficulties have to be overcome to include both time dependence and scattering. This normal mode reverberation method was first introduced by Bucker and Morris[8] and was developed in the some Chinese literature[45][35]. A bistatic shallowater sonar model based on normal modes has been developed and implemented by Ellis[12][10]. He showed that the the results from normal mode model are remarkable agreement with ray-based model. He showed that downward refracting sound-speed profile gives more bottom scattering than surface scattering because of the lower grazing angle. A distinct difference was noted from the different bottom properties, including high loss and low loss bottoms. He illustrated the analysis of bottom reverberation by modes.

He also summarized the merits and limits of other numerical models to solve scattering. There are several ray-based models of reverberation like RASP model[15], the Generic Sonar model[42] and MOCCASIN model[34] but all these models were developed to study deep water and are not adequate for shallow water because of the multipaths effects. Other approaches to the shallow-water reverberation problem are the angular spectrum method, parabolic equation methods and finite-difference techniques. The normal mode scattering is quite computationally efficient, easy to understand and easy to extend to other environments. The angular spectrum method can be used to extract backscattering strengths. Parabolic equation methods can deal with range dependence but not include the time dependence of the various paths. Finite-difference techniques are easy to implement for complicated envi-

ronments but computationally intense.

Essen[13] studied scattering from a rough sedimental seafloor containing shear and layering. A first-order perturbation approach based on the Born approximation was developed. For a shear-supporting or layered seafloor, both monostatic and bistatic scattering were considered where power law wave-number spectra was formed to be appropriate for backscattering rather than a Gaussian spectrum as used for sand or harder seafloor. For grazing angles below critical, shear-wave velocities faster than 350 m/s had an effect on scattered strength. For Lambert's rule, comparison with the experimental results is very simple and needs only one parameter of backscattering strength at normal incidence. But it cannot derive the physical process to relate backscattering strength to seafloor parameters.

Anand *et al.*[1] studied normal mode sound propagation in an ocean with random narrowband waves. The authors give an excellent review of random rough surface scattering, but they considered only limited environments such as an isovelocity ocean with random narrowband surface waves using perturbation theory.

Stephen *et al.*[37] developed the finite-difference method(FDM) for seismo-acoustic problems. FDM has several advantages such as versatility to include rigidity, body and interface waves, both forward and backward scatter, volume heterogeneity and a wide range of frequencies pulse beams at low grazing angles. It has disadvantages such as heavy computation and the difficulty of confirming accuracy for complex problems, which are quite crucial to the scattering computation. They pointed out that the scattered field from a rough and laterally heterogeneous seafloor is required to know the bottom-interacting ocean acoustics. Recent studies have shown that the physics of seafloor scattering can be quite complex with energy converting between waves in the water and seafloor. For a very rough, basalt seafloor, conversion of energy from compressional waves in the water to shear and interface waves at the seafloor is an important physical mechanism for generating strong backscatter. Unsed-

imented rough basalt has stronger backscatter at low grazing angles and at near normal angle. Another comment was that secondary scattering into interface waves(Stoneley and Scholte) is a loss mechanism with scattering converting into shear-body waves.

Rouseff and Ewart[30] studied the effect of random sea surface and bottom roughness on propagation in shallow water using the Parabolic Equation(PE) method. They showed that surface roughness is closely related to bottom scattering for sufficiently rough interfaces. They mentioned that volume randomness like soliton and solibores, turbulence, and sub-bottom inhomogeneities can affect the surface and bottom scattering. They insist that the lack of knowledge of the environment is more critical to simulate shallow water propagation than the quality of the acoustic modeling. In shallow water, the stochastic effects of the water column, bottom, sub-bottom, and the surface could easily dominate deterministic effects. Deep-water field experiments have shown that the environment plays the primary role in understanding acoustic propagation. Even for deep water, the stochastic ocean phenomena can dominate the deterministic features. They dealt with a simple scenario in the deep ocean but results are very interesting showing coupling between surface and bottom scattering.

Kuperman and Schmidt [22] [23] [33] developed a self-consistent scattering theory based on the wavenumber integral method to incorporate this theory into the OASES numerical code. They developed a boundary operator by perturbing the rotated boundary coordinate. This theory and code was developed to consider arbitrary elastic layers in the ocean bottom. Although this theory and code has many advantages, the heavy computation is inevitable especially in the long range. They concluded that the rough interface scattering conversion into shear waves contributes significantly to transmission loss. This theory will be reviewed in Chapter 2.

Tracey [40, 41] reformulated the K/S scattering theory into modal terms to make an

efficient code to calculate the scattered field in the waveguide. The scattered field calculated by the NMSCAT modal code is in good agreement with the one calculated by OASS, and has greater computationally efficiency. The modal approach is proven to be a good way to study scattering not only by computational efficiency but also by simplicity of scattering physics. The modal theory is easy extension to other environments i.e. range dependent problems. However Tracey didn't consider arbitrary elastic layers, only an elastic half space. This theory will also be reviewed in more detail in Chapter 2.

1.3 Contributions

The main result of this thesis is the development of a normal mode scattering theory and code which makes it possible to consider arbitrary elastic layers in the sub-bottom. Additionally, bottom scattering is studied for a shallow water waveguide using this numerical model. The normal mode scattering theory and code were originally developed by Tracey [40] and this thesis is an extension of his work. We developed the code as subroutines added to NMSCAT code as an option in order to use Tracey's integrated modal scattering code which can deal with rough surface scattering and volume scattering in the waveguide. Therefore all the options and statistics of NMSCAT can be used to combine with an option to consider arbitrary elastic layers.

We justify our study by showing how one elastic layer has a distinctive effect on the scattered field by comparing the scattered field from one limestone layer over a basalt half space to a limestone and a basalt half space case. We validate the results by comparing the scattered field by NMSCAT with the one by the OASS. There is at most a 2 dB difference in the scattered amplitude over all ranges and all depth in the water except at short ranges. The interference patterns over ranges and depths show very good agreement.

We also show the effects of layer thickness and bottom properties on the scattered field. For a 30 m thick limestone layer, the scattered field is maximized because the scattered field is driven by mode 6 which is resonant for this limestone layer. The interference pattern

reflects the 6th mode shape when we look at the scattered field vs. depth. We do not see these resonant phenomena in the mean field. We may infer from this that the modal approach can provide better experimental design through mode excitation of a particular mode to study scattering and easy understand of its physics. The scattered field can be a good tool to study bottom properties, because the scattered field is more sensitive to the bottom.

We investigate the effects of bottom properties on scattering by changing the sound speed and density. We used the same attenuation coefficient for all cases in order to avoid the illusion of overwhelming attenuation effects. The scattered fields resulting from different bottom properties are distinct, although there is not much difference in the mean fields. We might get more information by studying both the scattered and mean fields because they contain different information.

The extended NMSCAT can also model the bottom as a multiple elastic layered sub-bottom. This multiple layer model contains some assumptions and restrictions. The inability in computing the displacement and stress amplitudes of the mean field in the elastic layers by KRAKENC[29] leads to error in the scattered field because the mean field is used as a source of the scattered field. If we consider the thick elastic layer or high attenuation bottom type in the first or second layer which gives small errors in the mean field, the multiple elastic layer model then gives the quite accurate scattered field. This error could be easily corrected if a normal mode code like ORCA[43] is used to compute the mean field in the elastic layers.

Data based on measured bottom properties from the Korea Strait Experiment is used to study the scattering phenomena in shallow water. We model the bottom as 2 elastic layers over a moraine half space based on the experimental geoacoustic data. We study how the scattered field is affected by two uncertain parameters in the layered bottom. The two parameters are the thickness of the 1st elastic layer and the bottom properties of the second layer. The scattered fields by two parameters are distinct and different from the mean fields and are well explained by modal study. We also study the scattering by other parameters such as the sound speed profile, single mode excitation, cross-modal coherence,

and other parameters and statistics. We may infer from these results that the modal study of the scattered field may provide a good tool to study physics of scattering from the elastic bottom.

1.4 Organization

We review several related theories used for this thesis in Chapter 2. The normal mode theory for an unperturbed field is given first and followed by the rough surface scattering. After a brief mention of Kirchhoff theory and small perturbation theory, the K/S self-consistent perturbation scattering theory and modal formulation of this theory are summarized. Then we develop the generalized modal formulation of scattering in the water column considering arbitrary elastic layers over a half space.

In Chapter 3, we show the numerical results from modal theory developed in chapter 2 considering one elastic layer over a half space. We compare the results of the extended version of NMSCAT code with the ones of OASS. The effects of one elastic layer on the scattered field is shown. We study the effects of thickness and bottom properties of the elastic layer on the scattered field and continue to research the effects of other acoustic parameters on the scattered field.

The multiple elastic layered bottom is considered in Chapter 4. Some assumptions and restrictions are shown for computation of the scattered field considering multiple elastic layers. A comparison of the results with OASS results is given for two elastic layers and is followed for more elastic layers. A simulation of Korean experiment is given by modeling the sub-bottom as 3 elastic layers. We focus on the variations of the scattered fields by the first layer thickness and bottom properties of the second layer.

Finally, we summarize the work in this thesis and give some suggestions for future work in chapter 5.

Chapter 2

Scattering Theories

2.1 Overall

The title of this thesis '*Normal mode acoustic wave scattering considering elastic layers over a half space*' reflects theories such as normal mode, acoustic wave scattering, and their connection and relationship with elastic layers. The explanation is required to specify the terms and meaning and make it clear the objective of this thesis.

Wave scattering theory has ramifications such as volume scattering and surface scattering determined by the types of the scatterer considered. Volume scattering is produced by marine life and inhomogeneities of the ocean and the bottom. Surface scattering is applied to two dimensional distributions of scatterers, usually from sea surface and sea floor[14]. We will concentrate on the study of surface scattering from the ocean bottom in this thesis.

Rough surface scattering is usually studied by the approximate but tractable theories like Kirchhoff theory and perturbation theory, because the rigorous formal theories, such as integral equation techniques, variation methods, and Green's function approaches, lead to difficulties in application of realistic scenarios. Perturbation theory and and Kirchhoff theory have advantages to use numerical simulation techniques which become feasible in a few decade. These numerical techniques make it possible to determine the regimes of validity

of approximate theories and to extend to more realistic scattering problems[26]. We will use a self-consistent scattering theory which was based on the perturbation theory.

Scattering in a ocean waveguide is driven by the propagation of the mean field. The numerical models to compute the mean field are necessary to calculate the scattered field. There are several numerical methods to get the mean field in a waveguide, such as ray tracing, parabolic equation, wavenumber integral, and normal mode method*etc.*.

The wavenumber integral method is known to provide accurate reference solutions for evaluating the performance of new numerical models. This method also has the advantage of considering arbitrary fluid-elastic layers. Kuperman and Schmidt[22] extended OASES/SAFARI the wavenumber integral code, to compute the scattered field for any number of elastic layers. But this method requires many calculations, especially at long ranges since the computation time is a function of range. The efficiency of computation is quite important in modeling the scattered field because the scattered field usually requires heavy calculation.

The normal mode method is efficient for long ranges or low frequencies, because computation time depends on the number of modes but independent of range. Normal modes also give us an easy understanding of the physics of waveguide propagation and a sufficiently accurate solution for the mean field. The other advantage of this method is its relatively easy extension to consider range dependent environments. Recently, the theory and code to compute the scattered field by modal approach was developed by Tracey [40]. This modal approach is very efficient in computation time, but it can deal with only an elastic half space. In this thesis, we make a generalization of the normal mode scattering theory and code to consider arbitrary elastic layers with some restrictions.

A generalization of normal mode scattering is shown in this chapter. We begin with the normal mode theory to get the unperturbed field first. We then review rough surface scattering which includes small perturbation theory and the Kuperman and Schmidt(K/S) self-consistent scattering theory. Then normal mode theory is incorporated into the K/S scattering theory for the generalized normal mode scattering.

2.2 Normal Mode Theory for the Unperturbed Field

The method of normal modes is one of the significant methods to solve the wave equation and understand the physics of ocean acoustics in a waveguide. Since Pekeris [27] developed this method in the field of ocean acoustics, it is one of the preferred methods among many ocean acousticians because of several advantages. This theory was originally developed for range-independent environments and extended to handle range-dependent environments. Some normal mode code can deal with realistic sound speed profiles and multiple ducts, to model elastic bottom layers, to find seismic interface modes, and to model propagation at short ranges accurately. The modal theory has also been developed to handle geoacoustic inversion for wide ranges of environmental inputs and frequency bands[43].

Let us start from the derivation of the wave equation. The acoustic wave equation is derived from inviscid, compressible fluid mechanics without heat conduction using hydrodynamic equations. Euler's equation(Newton's 2nd law), the equation of mass conservation, and the adiabatic equation of state are linearized and incorporated to obtain a wave equation[16].

The standard wave equation is obtained from a linearized wave equation assuming ambient density $\rho(\vec{r})$ is constant and sound velocity $c_0(\vec{r})$ is independent of time.

$$\nabla^2 P(\vec{r},t) - \frac{1}{c_0^2(\vec{r})}\frac{\partial^2 P(\vec{r},t)}{\partial t^2} = 0 \tag{2.1}$$

where $P(\vec{r},t)$ is the excess acoustic pressure about the ambient pressure as a function of space and time and $c_0(\vec{r})$ is the sound velocity.

The time harmonic solution is assumed as $P(\vec{r},t) = p(\vec{r})e^{i\omega t}$ and is replaced in Eq. 2.1. If we assume the ocean waveguide is stratified horizontally and the sound velocity depends only on the depth, the wave equation including the source $f(\vec{r})$ is expressed as

$$[\nabla^2 + k_0^2(z)]p(\vec{r}) = f(\vec{r}) \tag{2.2}$$

where $k_0(z) = \frac{\omega}{c_0(z)}$ is the medium wave number at radial frequency ω.

For a plane wave problem within a two dimensional Cartesian coordinate system(x, z), the inhomogeneous Helmholtz equation for a line source at $(0, z_s)$ is

$$[\frac{\partial^2}{\partial x^2} + \frac{\partial^2}{\partial z^2} + k_0^2(z)]p(x,z) = -\delta(x)\delta(z - z_s) \tag{2.3}$$

The above equation can be transformed to the wave number domain by Fourier transform in order to reduce the dimension,

$$f(x,z) = \int_{-\infty}^{\infty} \tilde{f}(k,z)e^{-ikx}dk \tag{2.4}$$

$$\tilde{f}(k,z) = \frac{1}{2\pi}\int_{-\infty}^{\infty} f(x,z)e^{ikx}dx \tag{2.5}$$

Then the depth-separated wave equation with the depth-dependent Green's function which is defined as $\tilde{p}(k,z) = -\tilde{G}_w(k,z)$ is obtained with the boundary conditions in the spectral domain.

$$[\frac{\partial^2}{\partial z^2} + (k_0^2(z) - k^2)]\tilde{G}_w(k,z) = \frac{\delta(z - z_s)}{2\pi} \tag{2.6}$$

$$\tilde{B}[\tilde{p}(k,z_j)] = 0 \tag{2.7}$$

where B is the boundary operator and $j = 1, \cdots, N$ is the number of boundaries.

This depth-separated wave equation with the boundary conditions is an eigenvalue problem. The delta function can be expressed as a sum of modes and the Green's function is also a sum of modes

$$\delta(z - z_s) = \sum_m a_m \Psi_m(z) \tag{2.8}$$

$$\tilde{G}_w(k,z) = \sum_m b_m \Psi_m(z) \tag{2.9}$$

We can find the two coefficients a_m, b_m by applying the following integral operator and the orthogonality property.

$$\int_0^D (\cdot)\frac{\Psi_n(z)}{\rho(z)}dz \tag{2.10}$$

Finally, we can get Green's function after some algebra[19].

$$\tilde{G}_w(k,z) = \frac{1}{2\pi\rho(z_s)}\sum_m \frac{\Psi_m(z_s)\Psi_m(z)}{k^2 - k_m^2} \tag{2.11}$$

The above Green's function has singularities at k = $\pm k_m$.

If we take the inverse Fourier transform of the spectral Green's function, the pressure field in the spatial domain is obtained. We have to use Cauchy's theorem to evaluate the integral because the Green's function has simple poles at $k = \pm k_m$. The contour of the integral should be chosen in the lower half plane for the positive traveling waves since the traveling waves in the positive x direction are poles on the positive k axis. For attenuation of the waves, the complex wavenumber can be introduced but the imaginary part of the wavenumber must be negative in order to avoid the field blowing up as x goes to positive infinity for a positive k.

By this integral method, the pressure field is given by the sum of the residues of all poles and is normalized by the pressure at 1 meter.

$$p(x,z) = \frac{\sqrt{2\pi k_0}}{\rho(z_s)}e^{i(k_0-\pi/4)}\sum_m \frac{\Psi_m(z_s)\Psi_m(z)}{k_m}e^{-ik_m x} \tag{2.12}$$

The pressure field in cylindrical coordinates is obtained in a similar way. In the far field($kr \gg 1$), the asymptotic form of Hankel function is used and the normalized field is given

$$p(r,z) = \frac{1}{\rho(z_s)}\sqrt{\frac{2\pi}{r}}e^{i(k_0-\pi/4)}\sum_m \frac{\Psi_m(z_s)\Psi_m(z)}{k_m}e^{-ik_m r} \tag{2.13}$$

When the bottom is composed of elastic layers, we apply an impedance boundary condition. Even a simple Pekeris waveguide possesses the discrete spectrum which is a sum of proper modes, and the continuous spectrum which corresponds to leaky modes. The continuous spectrum is modeled by an approximate false bottom method by putting a pressure release boundary deep in the bottom in the normal mode theory. Both proper and leaky modes play an important role in rough surface scattering problems.

The mean field at the rough surface which can be calculated from normal mode theory is used as a source of scattering in the waveguide. We need to make a connection between normal mode theory and the scattering theory to formulate the normal mode scattering theory. Before we discuss the connection in detail, we summarize rough surface scattering theories.

2.3 Rough Surface Scattering

All surfaces in the real world are rough and the roughness causes scattering which is a function of frequency and angle of the incident wave. A random rough surface is usually described by two statistical functions, surface height distribution function and surface correlation function. From these functions, root mean square height and correlation length are determined, which are important parameters for representing the statistics of a random rough surface. The most widespread theories of scattering by statistically rough surfaces are the Kirchhoff method and the small perturbation method[2]. Before we follow the mathematical formula of the self-consistent scattering theory, we review briefly the two approximations, especially in regard to their validity and limitations.

The Kirchhoff theory has two main advantages for studying the scattering from rough surfaces: easily understandable physical basis and relatively simple analytical expressions

for the scattered field amplitudes. This theory assumes that any point on a scatterer is part of an infinite plane, parallel to the local surface tangent, which leads to en exact solution for an infinite, smooth, plane scatterer. The restrictions of Kirchhoff theory caused by these assumptions non self-consistency and lack of energy conservation. The latter arises through neglect of multiple scattering and propagating modes such as surface wave. The former leads to inaccurate calculation of the field away from points on the scatterer. In spite of the inaccuracies of the theory, Kirchhoff theory is one of the most widely used theories in the study of rough surface scattering. The accuracy usually depends on the shape and dimensions of the mean surface and the roughness of the surface. Since the Kirchhoff theory is not easy to extend to more complex environments, we will here use the self-consistent theory which is derived from the perturbation method after a brief review of the basic perturbation methods.

The basic idea of small perturbation method is that the boundary conditions at a rough surface can be transferred to the mean surface by expanding them into a powers of the roughness height. This method assumes that a rough surface deviates only slightly from a mean surface and has sufficiently small slopes, meaning,

$$k|\gamma(x,y)| \ll 1 \tag{2.14}$$

$$|\nabla\gamma(x,y)| \ll 1 \tag{2.15}$$

where k is the wavenumber of the incident wave and the $\gamma(x,y)$ is the height of the rough surface in 2 dimension. The mean surface usually assumes the plane which is zero height so that Taylor expansion can be applied. Then the perturbation method can be applied to study wave scattering. The foundation of wave scattering at a rough surface becomes equivalent to a radiation problem by the distribution of virtual sound sources.

The Rayleigh theory is an example of a perturbation approach. This theory was originally developed to calculate scattering from irregular sinusoidal rough surfaces. Later this was extended to deal with random rough surfaces. The scattered field is represented as a sum of outgoing plane waves. The coefficients in this summation are determined from the boundary

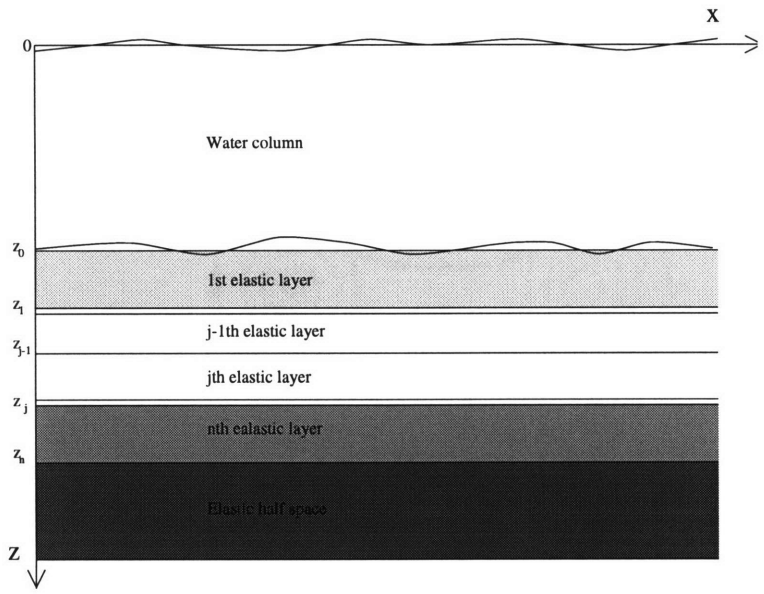

Figure 2-1: General shallow water scenario. Rough surface at the fluid-elastic interface.

conditions on the surface. The restrictions of this method are that multiple scattering effects cannot be considered because of the assumption of only outgoing scattered waves, and that only slightly rough surfaces can be solved because of the convergence of the series. The Rayleigh method is claimed to be good for periodic corrugated surfaces in the regime $0 < a\Lambda < 0.34$ and $0 < ka < 4.1$, where a is the amplitude of the surface corrugations, Λ is the surface period and k is the incident wave vector[44].

A self-consistent perturbation theory which is based on the perturbation theory is presented in detail in the next section.

2.4 Self-consistent Perturbation Scattering Theory

A self-consistent perturbation approach for normal mode propagation has been introduced by Kuperman and Ingenito[21] to incorporate rough surface scattering into the propagation problems. Kuperman and Schmidt[23] made a generalization of a self-consistent scattering theory to deal with arbitrary fluid or elastic rough interfaces in stratified fluid and

elastic layers. They combine the waveguide perturbation problem with Schmidt's elastic full-wave propagation[32] by which a boundary matrix operator is employed to make use of the OASES[31] algorithm for the unperturbed problem.

Let us summarize the K/S scattering theory in a two dimensional ocean for a one dimensional rough surface for simplicity. The boundary conditions are represented in a local rotated coordinate system on the rough surface since the rough surface has nonzero slope and finite curvature.

We will study the case of a rough surface is at the fluid-elastic interface(Fig. 2-1), but we will develop a generalized theory for a rough surface at an arbitrary interface.

If we assume the slope of the rough surface is small, the rotated boundary operator on the rough interface(at z_j) becomes,

$$B_j^*(p_j) \;=\; B_j(p_j) + \gamma' \circ b_j(p_j) \tag{2.16}$$

where γ is the surface height function and $\gamma' = \dfrac{\partial \gamma(x)}{\partial x}$ and $|\gamma'| \ll 1$ is assumed here. And the operator $\circ$ is the various vector operations.

The total field(p) is divided into coherent field($< p >$) and incoherent scattering field(s).

$$p_j \;=\; < p_j > + s_j \tag{2.17}$$

We insert Eq. 2.17 into Eq. 2.16 and expand Eq. 2.16 in a Taylor series around the rough interface(at z_j) to the second order in γ:

$$B_j^*(p_j) = (1 + \gamma\frac{\partial}{\partial z} + \frac{\gamma^2}{2}\frac{\partial^2}{\partial z^2})B_j^*(p_j)|_{z=z_j} + (1 + \gamma\frac{\partial}{\partial z})B_j^*(s_j)|_{z=z_j} \;= 0 \tag{2.18}$$

The scattered field is assumed to be order of γ and Eq. 2.18 is averaged over γ with the average properties of the operators $< B_j^*(< p_j >) >= B_j(< p_j >)$ and $< B_j(s_j) >= 0$.

$$< B_j^*(p_j) > = (1 + \frac{< \gamma^2 >}{2}\frac{\partial^2}{\partial z^2})B_j(< p_j >) + < \gamma' \circ b_j(s_j) > + < \gamma \frac{\partial B_j(s_j)}{\partial z} >$$
$$= 0 \tag{2.19}$$

If we take the difference between the above two equations Eq. 2.18 and Eq. 2.19, we get the boundary conditions for the scattered field,

$$B_j(s_j) + \gamma \frac{\partial B_j(< p_j >)}{\partial z} + \gamma' \circ b_j(< p_j >) = 0 \tag{2.20}$$

The surface correlation function $N(q)$ is used to solve the above equation with the stochastic variable of roughness. The surface roughness spectrum $P(q')$ is obtained by taking a Fourier transform of the correlation function,

$$N(q) = < \gamma(x')\gamma(x) > \tag{2.21}$$
$$< \gamma^2 > P(q') = \frac{1}{2\pi} \int N(q) e^{iq' \cdot q} d^2q \tag{2.22}$$

Performing a Fourier transform on Eq. 2.20 and applying some algebraic operations[23], the scattered field is as follows,

$$\tilde{B}_j(q)\tilde{s_j} = -\frac{1}{2\pi} \int \tilde{\gamma}(q-k)\tilde{T}_j(q,k) < \tilde{p_j}(k) > \tag{2.23}$$

, where

$$\tilde{T}_j(q,k) \equiv \left(\frac{\partial \tilde{B}(k)}{\partial z} - i(q-k) \cdot \tilde{b}(k) \right) \tag{2.24}$$

We can solve this equation by multiplying $\tilde{B_j}^{-1}(q)$ on both sides. $\tilde{B_j}$ is the global interface condition matrix and must be invertible.

Then a self-consistent boundary condition for the mean field is derived by Fourier transforming the equation for the mean field(Eq. 2.20) and inserting the solution of the above equation(Eq. 2.24), we then get the mean field equation as follows,

$$\left(\tilde{B}_j(k) + \frac{<\gamma^2>}{2}\frac{\partial^2 \tilde{B}_j(k)}{\partial z^2} + I_1(k) + I_2(k)\right) < p_j(k) > \ = 0 \tag{2.25}$$

where,

$$I_1(k) = -\frac{<\gamma^2>}{2\pi}\int d^2qP(q-k)\frac{\partial \tilde{B}_j(q)}{\partial z}\tilde{B}_j{}^{-1}(q)\tilde{T}_j(q,k) \tag{2.26}$$

$$I_2(k) = -\frac{<\gamma^2>}{2\pi}\int d^2qP(q-k)j(q-k)\cdot\tilde{b_j}(q)\tilde{B}_j{}^{-1}(q)\tilde{T}_j(q,k) \tag{2.27}$$

We can easily confirm that the above self-consistent boundary condition is the same with the mean field in Eq. 2.7 if we set $<\gamma^2>= 0$. The roughness of the surface acts as a damping force in the mean field. Self-consistent perturbation obviously does not require that we solve for the scattered field explicitly to calculate the mean field.

2.5 Modal Formulation of Kuperman/Schmidt Scattering Theory

Tracey[40] developed a modal formulation of K/S scattering theory. First we begin with a fluid-fluid rough interface in a two dimensional ocean and extend to the fluid-elastic boundary. The scattered field at some distance from the rough surface may be obtained by the incorporation of the effective field on a smooth surface into the source free Helmholtz integral formula[26] as

$$s(x,z) = \int_{S_0} dS_0[s(x_0,z_0)\frac{\partial G_w(x,z,|x_0,z_0)}{\partial n_0} - \frac{\partial s(x_0,z_0)}{\partial n_0}G_w(x,z,|x_0,z_0)] \tag{2.28}$$

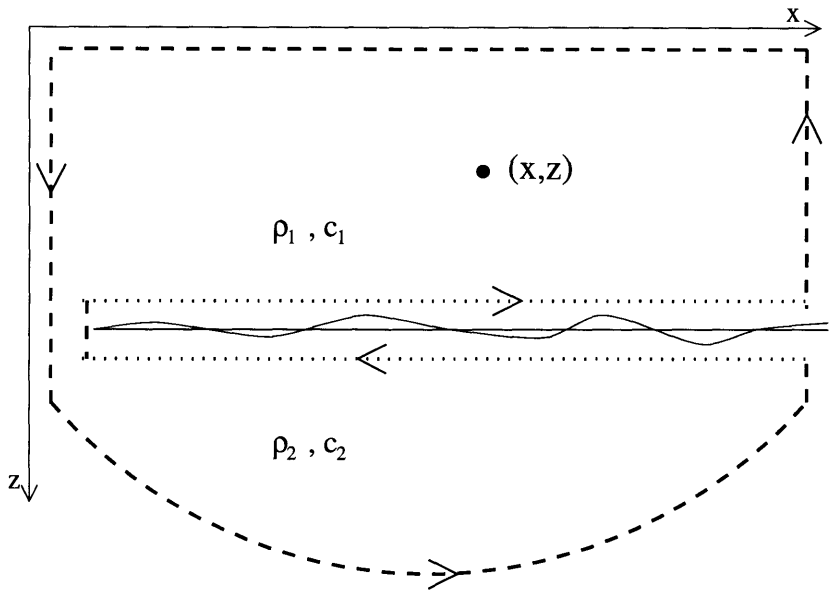

Figure 2-2: Helmholtz integral theorem for penetrable bottom. The surface integral is deformed to run along both sides of the rough surface(from Tracey,1996).

where n_0 is the unit outward normal to the scattering surface S_0, x_0, z_0 are the coordinates on the surface, $G_w(x, z|x_0, z_0)$ is the acoustic Green's function representing the effect at (x_0, z_0) of a point force at (x, z).

This is valid for all smooth surfaces but not valid for a rough surface since the Green's function is found for smooth interfaces. Therefore, the surface integral must be taken along the rough surface.

Taking a waveguide with a smooth surface and rough fluid-fluid bottom, the only line integral along the rough surface back and forth(dotted lines in Fig. 2-2) are to be used to get the scattered field. If the continuity and reciprocity of Green's functions are applied in the line integral to represent the field in the water, the scattered field is obtained as follows[40]

$$\begin{aligned} s(x,z) &= \int_{-\infty}^{\infty} dx_0[(s_1(x_0,z_0) - s_2(x_0,z_0))\frac{\partial G_w(x,z|x_0,z_0)}{\partial z_0} \\ &\quad -(\frac{\partial s_1(x_0,z_0)}{\partial z_0} - \frac{\rho_1}{\rho_2}\frac{\partial s_2(x_0,z_0)}{\partial z_0})G_w(x,z|x_0,z_0)] \end{aligned} \tag{2.29}$$

This equation means that the scattered field can be calculated from the discontinuities in the scattered field and its derivative at the rough surface. Taking the Fourier transform of the above equation, we obtain the wavenumber domain equation,

$$\tilde{s}(q,z) = 2\pi[\Delta_1(q)\frac{\partial \tilde{G}_w(q,z,z_0)}{\partial z_0} - \Delta_2(q)\tilde{G}_w(q,z,z_0)] \tag{2.30}$$

$$\Delta_1(q) \equiv \tilde{s_1}(q,z_0) - \tilde{s_2}(q,z_0) \tag{2.31}$$

$$\Delta_2(q) \equiv \frac{\partial \tilde{s_1}(q,z_0)}{\partial z_0} - \frac{\rho_1}{\rho_2}\frac{\partial \tilde{s_2}(q,z_0)}{\partial z_0} \tag{2.32}$$

where $\Delta_1(q)$ and $\Delta_2(q)$ are the discontinuity of the scattered field and momentum across the rough interface, respectively. This equation is for the fluid-fluid rough interface but it can be extended to a fluid-elastic rough interface after some complicated algebra involving the compressional and shear potentials.

Finally the scattered field can be given in the general form after applying K/S theory to find the forcing terms $\Delta_1(q)$ and $\Delta_2(q)$ and the incident field by modal sums. The result is

$$\tilde{s}(q,z) = \frac{1}{(2\pi)^2}\int_{-\infty}^{\infty} dk \sum_{m,n} \tilde{\gamma}(q-k)\Psi_n(z)\frac{a_{mn}(q,k)}{(k^2-k_m^2)(q^2-q_n^2)} \tag{2.33}$$

where

$$a_{mn}(q,k) \equiv \frac{-NM}{\rho(z_0)\rho(z)}[\Delta_m^{(1)}(q,k)\frac{\partial \Psi_n(z_0)}{\partial z_0} + \Delta_m^{(2)}(q,k)\Psi_n(z_0)] \tag{2.34}$$

NM is the normalized field at 1 m which comes from the normalized incident field. This equation tells us that the incident wave is driven by the scattered field.

In order to get the scattered field in the spatial domain, the inverse Fourier transform should be taken.

$$s(x,z) = \frac{1}{2\pi}\int_{-\infty}^{\infty} dq \tilde{s}(q,k)e^{-iqx}$$

$$= \frac{1}{(2\pi)^3} \iiint_{-\infty}^{\infty} dq dk dx_0 \sum_{m,n} \gamma(x_0) e^{i(q-k)x_0} \Psi_n(z) \frac{a_{mn}(q,k)}{(k^2-k_m^2)(q^2-q_n^2)} e^{-iqx} \quad (2.35)$$

The integrand has simple poles at $k = \pm k_m$ and $q = \pm q_n$ and the integrals over k and q can be calculated as a sum of residues using Cauchy's theorem. The positive poles are forward propagating waves and the negative poles are backward-propagating waves for both mean field and scattered field.

We can compute scattering only from the outgoing mean field of the source which means when $k = k_m$. Then the outgoing scattered field can be given by

$$s(x,z) = \frac{i}{(2\pi)^2} \int_{-\infty}^{\infty} dq \int_0^{\infty} dx_0 \sum_{m,n} \gamma(x_0) e^{-ik_m x_0} \Psi_n(z) \frac{a_{mn}(q,k_m)}{2k_m(q^2-q_m^2)} e^{-iq(x-x_0)} \quad (2.36)$$

Both forward($q = q_n$) and backward($q = -q_n$) scattering can be obtained from the above equation by applying the Cauchy's residue theorem for evaluating the integral.

2.6 Generalization of Modal Formulation for Arbitrary Elastic Layers

Tracey[41] developed a modal formulation consider only a half space elastic bottom. But his modal approach can be easily extended to consider arbitrary elastic layers below the fluid bottom over an elastic half space if we want to know the field in the fluid. Although the algebra is somewhat complicated, the theoretical idea and approach are almost the same. Let us consider a 2 dimensional waveguide with N elastic layers below the water column over a half space, Fig. 2-1. We assume the rough surface is at the fluid-elastic interface for the first step.

The field in the j-th elastic layer has the Helmholtz integral representation with the time harmonic dependence $e^{i\omega t}$ under the assumption of plain strain with Lame constants λ_j, μ_j. Using local coordinate system to avoid the instability to solve global matrix, the

compressional and shear wave fields are written as,

$$\phi_j(x,z) = \int_{-\infty}^{\infty} [\tilde{\phi}_j^-(k)e^{-\alpha_j(z-z_{j-1})} + \tilde{\phi}_j^+(k)e^{\alpha_j z(z_j-z)}]e^{-ikx}dk \quad (2.37)$$

$$\psi_j(x,z) = \int_{-\infty}^{\infty} [\tilde{\psi}_j^-(k)e^{-\beta_j(z-z_{j-1})} + \tilde{\psi}_j^+(k)e^{\beta_j(z_j-z)}]e^{-ikx}dk \quad (2.38)$$

where $\alpha_j = \sqrt{k^2 - k_{pj}^2}$ and $\beta_j = \sqrt{k^2 - k_{sj}^2}$ with k_{pj} and k_{sj} are the compressional and shear wavenumbers, respectively. The superscript + and - represent up-going and down-going wave components, respectively.

Since the fluid doesn't support shear waves, we can neglect the second equation in the water column.

$$\phi(x,z) = \int_{-\infty}^{\infty} [\tilde{\phi}^-(k)e^{-\alpha_0 z} + \tilde{\phi}^+(k)e^{\alpha_0 z}]e^{-ikx}dk \quad (2.39)$$

where $\alpha_0 = \sqrt{k^2 - k_0^2}$ with k_0 the compressional wavenumber.

In the elastic half space, the upgoing waves don't exist because the down-going waves never return. Then the half space field can be given as,

$$\phi_n(x,z) = \int_{-\infty}^{\infty} \tilde{\phi_n^-}(k)e^{-\alpha_n(z-z_{n-1})}e^{-ikx}dk \quad (2.40)$$

$$\psi_n(x,z) = \int_{-\infty}^{\infty} \tilde{\psi_n^-}(k)e^{-\beta_n(z-z_{n-1})}e^{-ikx}dk \quad (2.41)$$

We can get displacement and stress relationship[5] in the j-th layer which can be represented as a matrix,

$$\begin{bmatrix} \tilde{u}_j(k,z) \\ \tilde{w}_j(k,z) \\ \tilde{\sigma}_{zzj}(k,z) \\ \tilde{\sigma}_{xzj}(k,z) \\ \tilde{\sigma}_{xxj}(k,z) - \tilde{\sigma}_{zzj}(k,z) \end{bmatrix} = \begin{bmatrix} -ik & -ik & \beta_j & -\beta_j \\ -\alpha_j & \alpha_j & -ik & -ik \\ \mu_j(2k^2 - k_{si}^2) & \mu_j(2k^2 - k_{si}^2) & 2i\mu_j k\beta_j & -2i\mu_j k\beta_j \\ 2i\mu_j k\alpha_j & -2i\mu_j k\alpha_j & -\mu_j(2k^2 - k_{si}^2) & \mu_j(2k^2 - k_{si}^2) \\ 2\mu_j(2k^2 - k_{pi}^2) & 2\mu_j(2k^2 - k_{pi}^2) & 4i\mu_j k\beta_j & -4i\mu_j k\beta_j \end{bmatrix} \times \begin{bmatrix} \tilde{\phi}_j^-(k)e^{-\alpha_j(z-z_{j-1})} \\ \tilde{\phi}_j^+(k)e^{-\alpha_j(z_j-z)} \\ \tilde{\psi}_j^-(k)e^{-\beta_j(z-z_{j-1})} \\ \tilde{\psi}_j^+(k)e^{-\beta_j(z_j-z)} \end{bmatrix} \quad (2.42)$$

The boundary conditions must be satisfied at all boundaries with the kernels in the integral representations. There are 4 boundary conditions between two elastic layers. They are continuity of normal stress σ_{zz}, tangential stress σ_{xz}, horizontal displacement u, and vertical displacement w. Three boundary conditions must be satisfied at the fluid-elastic interface. The normal stress in the elastic layer must be equal with the negative pressure in the fluid which is expressed as $\sigma_{zz} = -p_w$. The continuity of vertical displacement is expressed by $\omega^2 w = \frac{1}{\rho_0}\frac{\partial p_w}{\partial z}$. And no tangential stress $\sigma_{xz} = 0$.

For a $n+1$ layered waveguide including half space, the $4n+2$ unknown wave-field amplitudes in the elastic layers with one known mean field($\Psi_m(z_0,k)$) at the fluid bottom interface can be collected in a column vector.

$$\tilde{p}(k) = \begin{bmatrix} \Psi_m(z_0,k) \\ \tilde{\phi}_1^{\mp}(k) \\ \tilde{\psi}_1^{\mp}(k) \\ \vdots \\ \tilde{\phi}_n^-(k) \\ \tilde{\psi}_n^-(k) \end{bmatrix} \quad (2.43)$$

,where Ψ_m is the modal value of the field at the fluid-elastic interface.

Then the global boundary matrix $\tilde{B}$ becomes 4n+3 square matrix to satisfy the all boundary conditions.

$$\tilde{B} = \begin{bmatrix} \begin{pmatrix} 1 \\ \frac{1}{\rho_0}\frac{\partial}{\partial z} \\ 0 \end{pmatrix} & \begin{pmatrix} 3\times 4 \end{pmatrix} & \bigcirc & \cdots & \bigcirc \\ 0 & \begin{pmatrix} 4\times 4 \end{pmatrix} & \begin{pmatrix} 4\times 4 \end{pmatrix} & \cdots & \bigcirc \\ 0 & \bigcirc & \begin{pmatrix} 4\times 4 \end{pmatrix} & \cdots & \bigcirc \\ \vdots & \vdots & \vdots & \vdots & \vdots \\ 0 & \bigcirc & \bigcirc & \begin{pmatrix} 4\times 4 \end{pmatrix} & \begin{pmatrix} 4\times 2 \end{pmatrix} \end{bmatrix} \tag{2.44}$$

,where $\bigcirc$ is 4×4(4×2 for the last column) zero matrices. The other matrix components can be obtained by the boundary matrix given Eq. 2.42.

The depth derivation of boundary matrix($\frac{\partial \tilde{B}}{\partial z}$) can be obtained by multiplying the columns $\frac{\partial}{\partial z}, -\alpha_1, -\beta_1, \alpha_1, \beta_1, \ldots, -\alpha_n, -\beta_n$.

The rotation operator $\tilde{b}(k)$ can also be derived in a similar way from the field parameter discontinuities. They are the horizontal and vertical displacement discontinuities, tangential stress discontinuity, and the discontinuity of differences of two normal stresses for the elastic interface.

$$\tilde{b}_j(k) = \begin{Bmatrix} -\tilde{u}_{x:j} + \tilde{u}_{x:j+1} \\ \tilde{w}_{x:j} - \tilde{w}_{x:j+1} \\ -2\tilde{\sigma}_{xz:j} + 2\tilde{\sigma}_{xz:j+1} \\ \tilde{\sigma}_{zz:j} - \tilde{\sigma}_{xx:j} - \tilde{\sigma}_{zz:j+1} + \tilde{\sigma}_{xx:j+1} \end{Bmatrix} \tag{2.45}$$

For the fluid-elastic interface, the discontinuity of the vertical displacement is removed for two-dimensional P-SV propagation in one-dimensional rough surface.

The depth derivative of boundary matrix and the rotation operator are used in the K/S

equation[23]. The incident mean field is written as a sum over modes m and it is used as a source of scattered field,

$$\begin{aligned}
\tilde{B}(q)\tilde{s}(q) &= \frac{-NM}{(2\pi)^2\rho(z_s)}\int_0^\infty dk \sum_m \tilde{\gamma}(q-k)\frac{\Psi_m(z_s)}{k^2-k_m^2} \\
&\quad \times \left[\frac{\partial \tilde{B}(k)}{\partial z} - i(q-k)\tilde{b}(k)\right] \begin{bmatrix} \Psi_m(z_0) \\ \tilde{\phi}_{1m}^{\mp} \\ \tilde{\psi}_{1m}^{\mp} \\ \vdots \\ \tilde{\phi}_{nm}^{-} \\ \tilde{\psi}_{nm}^{-} \end{bmatrix} \qquad (2.46) \\
&\equiv \frac{-NM}{(2\pi)^2\rho(z_s)}\int_0^\infty dk \sum_m \tilde{\gamma}(q-k) \begin{bmatrix} a_m^{(11)}(q,k) \\ a_m^{(12)}(q,k) \\ a_m^{(13)}(q,k) \\ 0 \\ \vdots \\ 0 \end{bmatrix} \text{ or } \begin{bmatrix} \vdots \\ a_m^{(j1)}(q,k) \\ a_m^{(j2)}(q,k) \\ a_m^{(j3)}(q,k) \\ a_m^{(j4)}(q,k) \\ \vdots \end{bmatrix} \qquad (2.47)
\end{aligned}$$

where $\tilde{\phi}_{jm}^{\mp}, \tilde{\psi}_{jm}^{\mp}$ are the mean field amplitudes by modes in the j-th elastic layer. They are the up- and down-going wave components for compressional and shear stress waves in the j-th layer. The best way to get these components is from a normal mode code like ORCA[43] which can give the field value in any elastic layers. However we use KRAKENC[29] to get the value of $\Psi_m(z_0, k)$, because ORCA code was not available at the initiation of this work. KRAKENC cannot compute the other wave components in the elastic layers.

We must compute these unknown coefficients by modes in the elastic layers to solve the equation Eq. 2.46. We can compute them by solving the mean field boundary conditions, $\tilde{B}\tilde{p} = 0$ combining Eq.2.43 and 2.44. There are $4n+2$ unknown coefficients but $4n+3$ equations in this matrix equation. We neglect the 2nd row in the matrix equation to minimize errors from the depth derivation in order to solve this matrix equation. Then we make a

$4n+2$ square matrix by moving $\Psi_m(z_0,k))$ term which is given by KRAKENC to the right hand side of the matrix equation. If we solve the matrix equation with the source $\Psi_m(z_0,k)$, we can get the modal coefficients of up- and down-going waves in elastic layers. We usually encounter a floating point error to solve this matrix equation through a standard matrix solver when two or more layers are considered. Therefore we cannot get the exact mean fields by modes for many elastic layers using KRAKENC. However this approach to solve the matrix equation can sill be applied with some approximations. We will discuss this in detail in Chapter 4.

The terms like $a_m^{(11,12,13)}$ in Eq. 2.47 are the sum of all mean field components which are used as a source of scattering from one rough surface in the scattering equation(Eq. 2.47). But up- and down-going wave components in the first layer dominate the other components in the layers below. Therefore we can use only these dominant components of the mean field as a source in the scattering equation even when we consider many layers. Generally, this approximation works well with some limitations which we will examine in detail in Chapter 4.

The rough surface has so far been assumed to be only at the fluid-elastic interface. We can easily have roughness at an arbitrary elastic interface if a normal mode code to solve for the mean fields in elastic layers were available. If the amplitude of up- and down-going waves in the elastic layers is obtained by modal code, a_m^{j1-4} at the j-th rough surface in Eq. 2.47 can be calculated. We don't consider this case because the modal code was not available to us at the initial stage of this work.

If we solve the scattering equation(Eq. 2.47), we can get the impedance form of the equation with unknowns of the scattered field in the fluid.

$$\tilde{s}(q,z_0) - Z_0(q)\frac{\partial \tilde{s}(q,z_0)}{\partial z} = R_s(q) \tag{2.48}$$

where,

$$Z_0(q) \equiv -\frac{\mu}{\rho_1 \omega^2} \frac{(2q^2 - k_s^2)^2 - 4q^2\alpha(q)\beta(q)}{\alpha(q)k_s^2} \tag{2.49}$$

and

$$R_s(q) \equiv \frac{-NM}{(2\pi)^2 \rho(z_s)} \int_0^\infty dk \sum_m \tilde{\gamma}(q-k) \frac{\Delta_m^{(1)}(q,k) + \Delta_m^{(2)}(q,k) Z_0(q)}{k^2 - k_m^2} \tag{2.50}$$

where

$$\Delta_m^{(1)} \equiv a_m^{(11)}(q,k) + \frac{iqa_m^{(13)}}{\alpha(q)k_s^2}(2q^2 - k_s^2 - 2\alpha(q)\beta(q)) \tag{2.51}$$

$$\Delta_m^{(2)} \equiv -\rho_1 a_m^{(12)}(q,k) \tag{2.52}$$

$\tilde{s}(q, z_0)$ is the scattered field in the fluid-elastic rough surface and the $R_s(q)$ is the forcing term.

A wavenumber domain solution to this equation can be written down following Kudryashov [20]

$$\tilde{s}(q,z) = \frac{R_s(q)\Psi(q,z)}{\pi(q)} \tag{2.53}$$

$$\pi(q) = \tilde{s}(q,z_0) - Z_0(q)\frac{\partial \tilde{s}(q,z_0)}{\partial z} \tag{2.54}$$

Transforming to the spatial domain and summing of the residues for the forward-scattering poles $q = q_n$, the forward scattered field is given by

$$s_f(x,z) = \frac{NM}{2\pi\rho(z_s)} \int_0^x dx_0 \sum_{m,n} \gamma(x_0) e^{i(q_n - k_m)x_0} \frac{\Psi_n(z)}{2q_n} \tag{2.55}$$

$$\times \frac{[\Delta_m^{(1)}(q_n,k_m)\frac{\partial \Psi_n(z_0)}{\partial z} + \Delta_m^{(2)}(q_n,k_m)\Psi_n(z_0)]}{2k_m} e^{-iq_n x} \tag{2.56}$$

and the backscattered field($q = -q_n$) at the source range is written as,

$$s_b(0,z) = \frac{NM}{2\pi\rho(z_s)} \int_{-\infty}^{\infty} dx_0 \sum_{m,n} \gamma(x_0) e^{i(-q_n - k_m)x_0} \frac{\Psi_n(z)}{-2q_n} \tag{2.57}$$

$$\times \frac{[\Delta_m^{(1)}(-q_n, k_m)\frac{\partial \Psi_n(z_0)}{\partial z} + \Delta_m^{(2)}(-q_n, k_m)\Psi_n(z_0)]}{2k_m} e^{-iq_n x} \tag{2.58}$$

These two equations are the same as the equations for a fluid-fluid rough surface in Eq. 2.35 and 2.36. Therefore the two procedures are proven to be the same.

Therefore all Tracey's formula and code including statistics in his thesis[40] can be used to study scattering in a waveguide by developing subroutines which incorporate elastic layers in his NMSCAT modal code.

We will study scattering in a shallow water waveguide by this modified NMSCAT code in the following chapters.

Chapter 3

Scattering Considering an Elastic Layer Over a Half Space

In this chapter, the theory developed in Chapter 2 is implemented demonstrated. The code NMSCAT which was originally developed by Tracey[40] is extended to deal with multiple elastic layers in the bottom. Parameter studies in surface and volume scattering were shown in Tracey's work for a fluid, a rigid and an elastic half space. Since the basic theory is the same even when the elastic layers are considered, the extended code should be able to reproduce Tracey's results.

We will not repeat all Tracey's parameter and statistical studies of coherence here. Instead we will concentrate on rough bottom scattering. We will study how the elastic layers affect rough surface scattering by modal analysis.

We will show numerical results of the extended version of NMSCAT considering only one elastic layer over a half space in this chapter. First, a comparison with the reference solution from OASS will be given to show the accuracy of the modal approach calculating rough surface scattering from a bottom with a single elastic layer over a half space. We will show differences of the scattered field between one layered bottom model and a half space bottom model. The effects of an elastic layer on the scattering will be studied by varying some

acoustic parameters, like thickness, density and sound speed. The studies of scattering will be presented using modal concepts.

3.1 Comparison with OASS Model

The first test case scenario has a limestone elastic layer over a basalt half space as shown in Fig. 3-1. The fluid-elastic interface is rough and the lower interface is smooth to avoid multiple scattering. The sound speed in the water is constant. The sound speeds and the densities of the limestone and basalt are taken from Computational Ocean Acoustics[19]. The attenuation coefficients are 0.1 dB/λ for the compressional wave and 0.2 dB/λ for the shear wave for both limestone and basalt. Real sediments in shallow water are usually composed of clay, silt or sand for the first layer and moraine and chalk for the subbottom although this varies regionally. These bottom types are relatively soft compared with limestone or basalt. There are several reasons for a limestone-basalt bottom to be considered. One is for convenience to compare the results with previous work by others. The field scattered by hard bottom is usually so strong that we can magnify the effects of scattering by each parameter, giving a more clear and distinct understanding. The interface waves are also easily identified and studied.

Fig. 3-2 shows the results of two numerical models. The RMS height and correlation length is 1 m and 20 m, respectively at the fluid-elastic rough surface. A Goff-Jordan[17] roughness spectrum is assumed. The Goff-Jordan spectrum and one of its realizations are shown in Appendix A to be compared with Guassina spectrum. The thickness of the limestone elastic layer is 20 m. A point source in 2 dimensional ocean is at 50 m depth and the frequency is 50 Hz. The expected scattered intensities are shown in Fig. 3-2 as a function of range for a receiver at 50 m depth. The solid line is the result from the OASS code and the dashed line is the result from the NMSCAT. The expected scattered field intensity has the same interference pattern over all ranges and is within 2dB except at short range. The accuracy of the scattered intensity at short range is known to be dependent on the ability

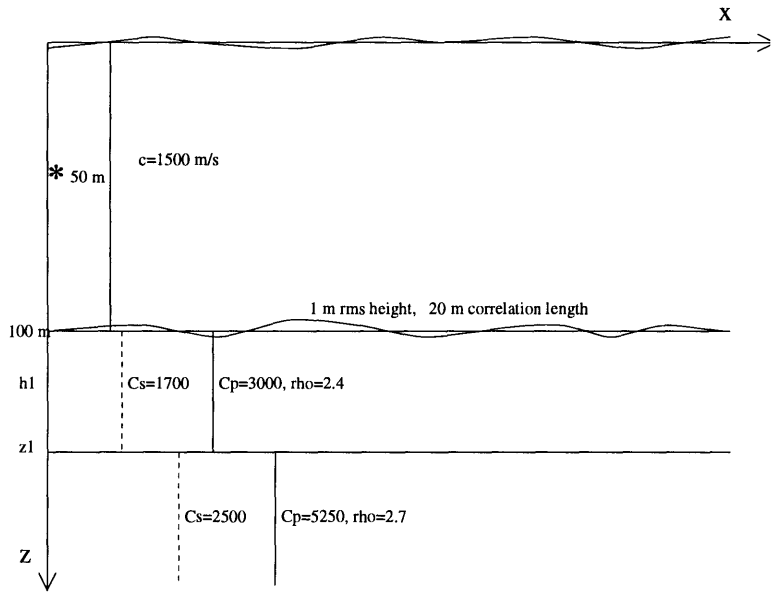

Figure 3-1: One elastic layer scenario–limestone layer over basalt half space.

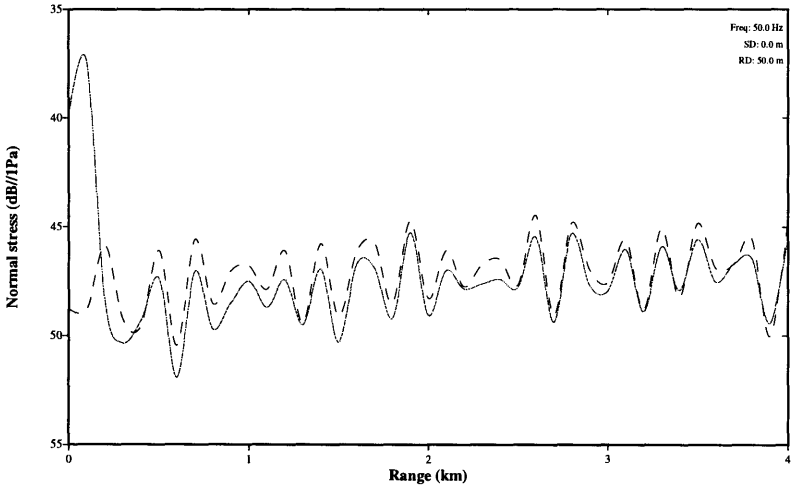

Figure 3-2: Comparison of results from OASS and NMSCAT. 20 m thick limestone over basalt half space. The solid line is from OASS and the dashed line is from NMSCAT.

to model the continuous spectrum. The normal mode model has inherent errors in modeling the scattered field at short range because normal mode theory cannot calculate continuous spectrum correctly. Other possibilities of error might lie in the computation of the modal derivative of the mean field at the rough surface and the modal displacement and stress components in the elastic layers because the scattered field is very sensitive to the mean field. But this error should be very small in the one elastic layer scenario. We will look at this error in more detail later when multiple layers are considered in Chapter 4.

Fig. 3-3 shows the scattered field as a function of depth and range from OASS and NMSCAT. These two results are almost the same both in amplitude and interference pattern except near the source. The amplitude differences are smaller than 3 dB over all range and depth. The high amplitudes near the bottom are due to the Scholte wave. It decays rapidly in the depth direction so that we can observe these interfacial wave effects only within 10 m from the bottom at this frequency.

We can conclude from these agreements that the NMSCAT code provides a good approximation to the scattered field. The efficiency in computation time is shown in Tracey's thesis[40] and this trend is the same in this extended version of NMSCAT because the modal code is dependent only on the number of modes.

3.2 The Effects of an Elastic Layer

Real ocean bottoms are often composed of several elastic layers. Most elastic layers have inhomogeneities with random roughness but are generally thought of as horizontally stratified. The scattered field is strongly influenced by the acoustic parameters of these elastic layers and roughness statistics. The roughness statistics have been studied by many scientists[6][18][26].

The waves scattered from a rough surface propagate through the elastic bottom layers and interact with the elastic interfaces and layers. When we model the bottom as an elastic half-space, we neglect any possible layers below the first elastic interface and therefore expect errors in the predicted acoustic field.

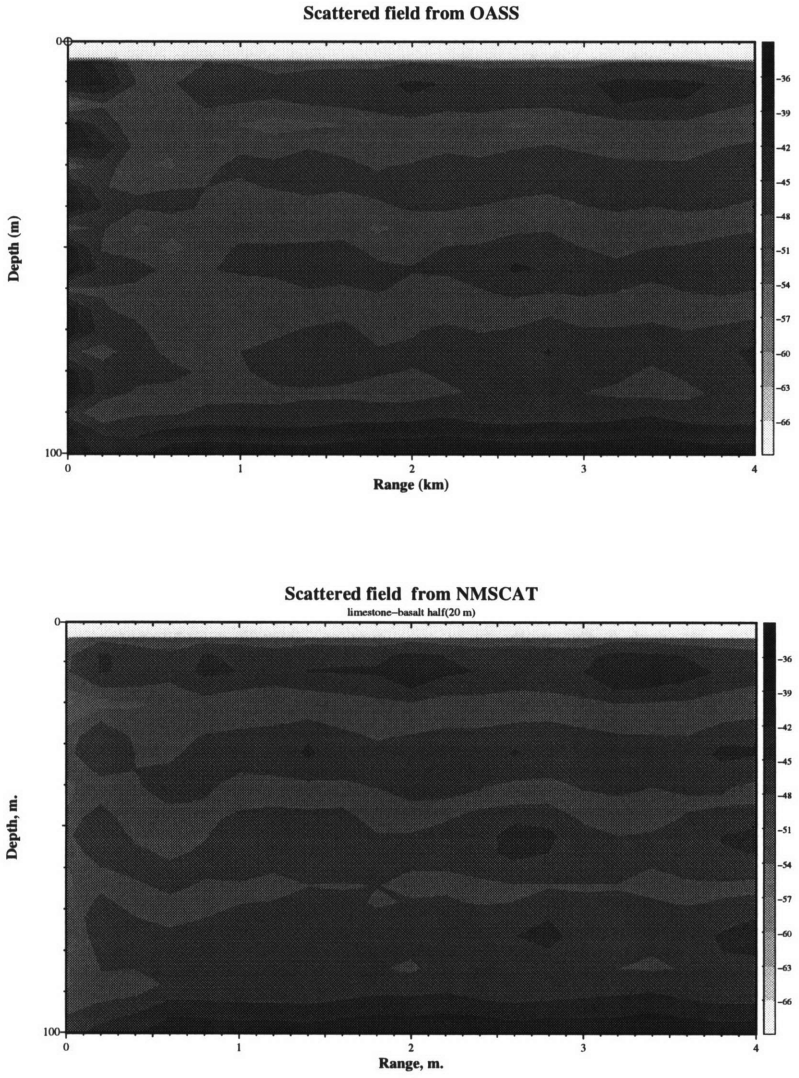

Figure 3-3: Comparison of results from OASS and NMSCAT. The upper picture is from OASS and the lower picture is from NMSCAT. Same scenario as Fig. 3-2.

In this section, we will study how much one elastic layer affects the scattered field. We assume that only the fluid-elastic layer is rough and the other lower layers are smooth, which means that the source of the scattered field is only from that rough surface.

Fig. 3-4 shows the scattered fields calculated from a limestone half space(solid line) and a basalt half space(dashed line) and one 10 m limestone layer over a basalt half space(dotted line). The magnitude of the scattered field from one layer model is higher than the one from the limestone half space, and smaller than the one from the basalt half space except at very short range. The intensity of the scattered field is similar to that from the basalt half space near the source but it becomes similar to that of the limestone half space at long range. At short range, the waves enter into the bottom at steep angles. The steep-angle waves are not affected strongly by the limestone layer because its thickness is shorter than one wave length(30 m). The specular angles from the first and second interfaces are almost the same when the angles are steep. Therefore we can see strong intensity at short range because the scattered waves from the 1st interface are added constructively to the reflected waves from the second interface. But at long ranges, the incident grazing angles at the rough surface become lower. Then the field in the limestone becomes more evanescent and consequently does not see the basalt. Therefore, the scattered field becomes similar to the scattered field from a limestone half space.

The interference patterns are different from one another although the one layer model may become similar to the limestone half space at long range. These interference and phase differences are thought to be related to the thickness of the limestone layer, the incident angles of the wave, the acoustical parameters, and coupling effects of two elastic layers.

From these distinct differences in the expected scattered fields, we can conclude that incorporating the effects of a layer can dramatically affect the scattered field. These effects include the interactions of scattered and scattered-reflected waves from two interfaces. This is the reason we should model the bottom as multiple layered for more realistic and accurate scattered. One can conjecture that the inclusion of more layers in the model will also significantly enhance scattered field predictions in realistic layered bottoms.

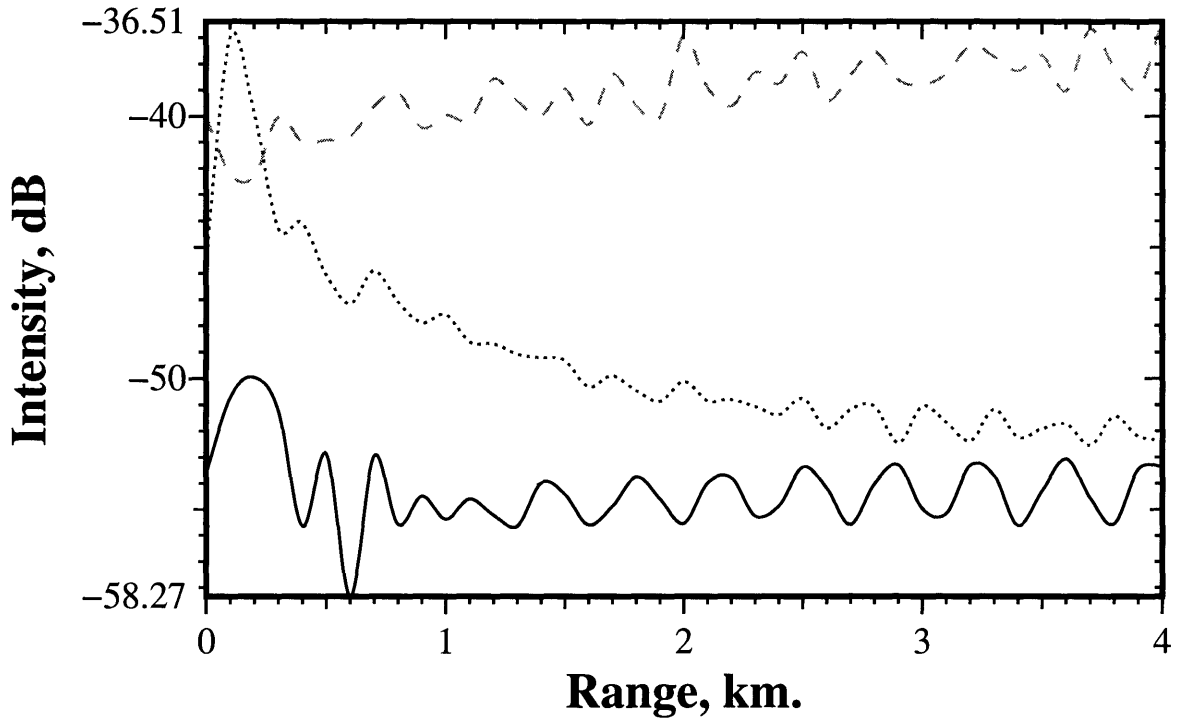

Figure 3-4: Effect of an elastic layer on the expected scattered field at z=50 m. The solid line is from the limestone half space, the dashed line is from the basalt half space, and the dotted line is from one limestone layer(h=10 m) over a basalt half space. The other parameters are the same as in Fig. 3-1.

3.3 Thickness Effects

We have examined how one elastic layer affects the scattered field in the previous section as a validation of our efforts in extending Tracey's NMSCAT code. Now we move to the effects of the thickness of the elastic layer.

Fig. 3-5 shows the expected scattered field intensity as a function of range and thickness of the elastic layer. All the environmental parameters are the same as in the scenario shown in Fig. 3-1 except the depth of the second interface which is varied. The maximum intensity of the scattered field appears at a thickness of 30 m except near the source. The scattered field converges to scattering from a limestone half space as the thickness becomes more than 10 wavelengths($\lambda = 30m$). If we consider that the attenuation coefficients of compressional and shear waves are 0.1 and 0.2 dB/λ, respectively, this is what we expect.

We investigate the 30 m case in more detail in Fig. 3-6. The scattered field shows the distinct modal pattern in the depth direction. Looking at the mode shapes in the lower picture, we see that the 6th mode shape is the same as the modal pattern of the scattered field. The 6th mode corresponds to an incident angle of about 22.2^o . The waves incident on the limestone layer at 22.2^o angle resonate with the reflected waves from the basalt half space. This resonant mode in the limestone layer strongly excites scattering to give the maximum intensity. We can easily observe this resonant phenomenon in the the 6th mode shape in the limestone layer. Therefore the scattered field is dominated by mode 6. This explanation by mode shapes makes understanding of the scattered field easy. It is one of the advantages of the normal mode approach.

Interestingly, we cannot observe these phenomena in the mean field; there are only phase differences as shown in Fig. 3-7.

We can infer from these facts that the scattered field is a good way to study the thickness of the elastic layer because the scattered field is much more sensitive to changes in the depth of the elastic layer. Further, a modal approach is an intuitive way to explain the physics of the scattered field.

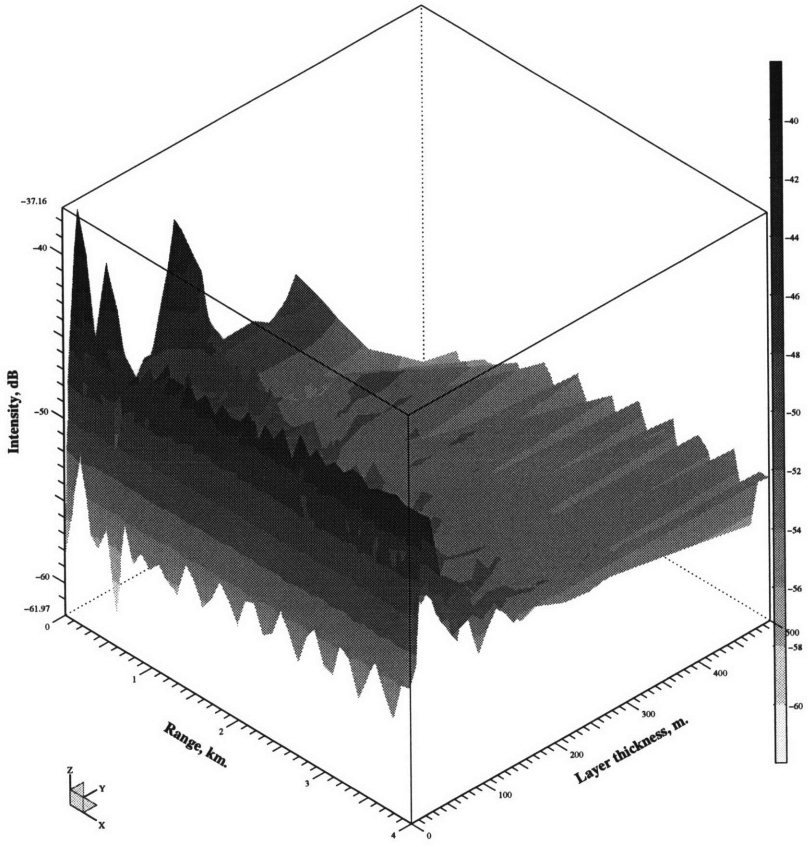

Figure 3-5: Effect of thickness of one elastic layer on the scattered field at the receiver z=50 m.

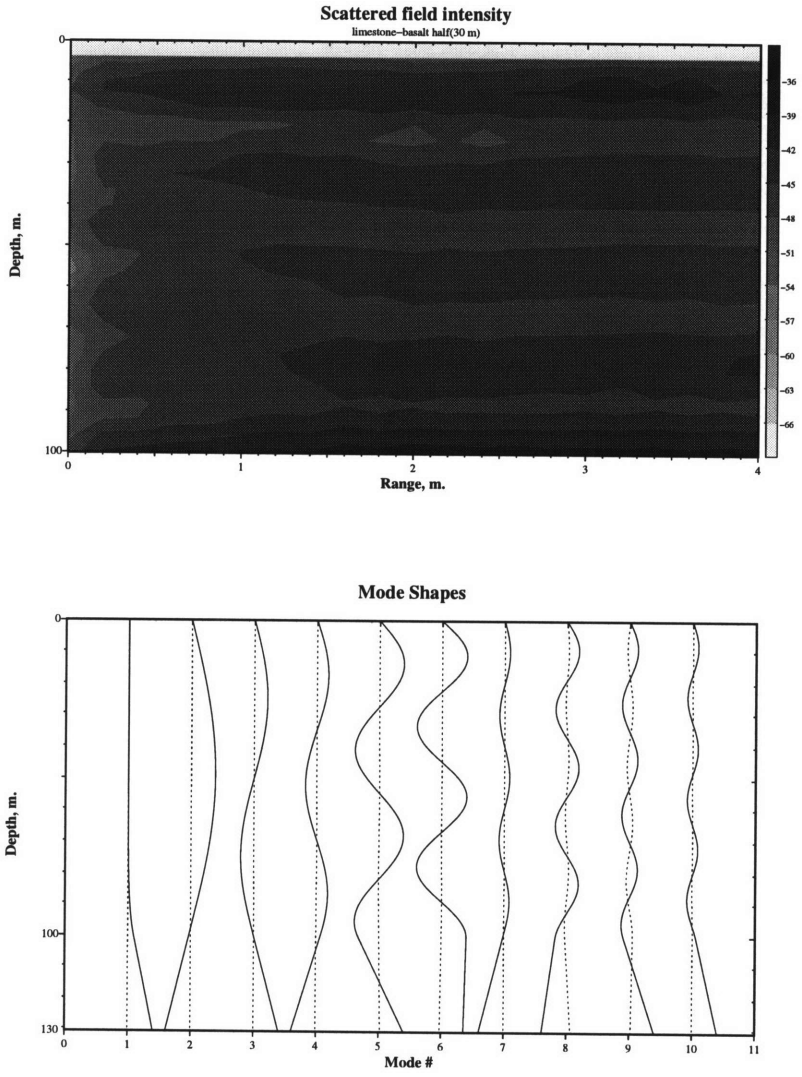

Figure 3-6: Scattered field and mode shapes of a 30 m limestone layer over a basalt half space. The same with the scenario as in Fig. 3-1 for other parameters. The 1st mode is a Scholte wave and 6 modes from 2nd to 7th mode are proper modes and the other modes are leaky modes.

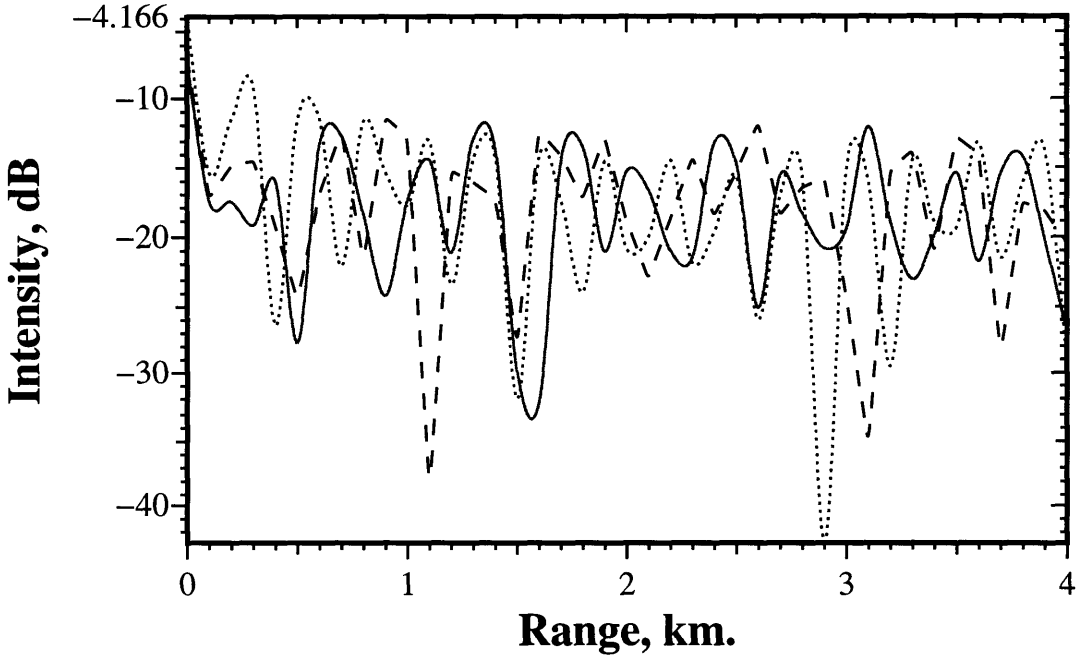

Figure 3-7: Mean field for different thickness of the 1st layer. The solid line is for 30 m, the dashed line is for 20 m, and the dotted line is for 10 m.

Table 3.1: Geoacoustic properties of three different elastic layers.

Bottom type	*Density*(g/cm^3)	c_p(m/s)	c_s(m/s)	$\alpha_p(dB/\lambda)$	$\alpha_s(dB/\lambda)$
Moraine	2.1	1950	600	0.1	0.2
Chalk	2.2	2400	1000	0.1	0.2
Limestone	2.4	3000	1700	0.1	0.2
Basalt	2.7	5250	2500	0.1	0.2

3.4 The Effects of Bottom Properties

We have shown the effect of layer thickness on the scattered field in the last section. Now we will examine how the different properties of the elastic layer affect the scattered field.

In order to determine the effects of bottom properties, the elastic layer thickness is set to 30 m in this section. The acoustic parameters for the materials of each elastic layer are taken from Computational Ocean Acoustics[19] and are shown in Table 3.1. We use the same attenuation coefficient(0.1 and 0.2 dB/λ for compressional and shear wave, respectively) to avoid effects of the attenuation. The attenuation affects the scattering very strongly but these effects may be linearly added because the attenuation is a linear function of range and the coefficients[4].

Fig. 3-8 and Fig. 3-9 are the mean and scattered intensities,respectively, for different acoustic properties. The solid line is for the limestone layer, the dashed line is for the chalk layer, and the dotted line is for the moraine layer.

We can easily observe that the trends of the scattered fields are different from the ones of the mean fields. The limestone and moraine layers(solid and dotted line, respectively) give almost the same intensity over all ranges in the mean field although the interference pattern is different. In the scattered field, the fluctuations of the dotted line(moraine layer) is bigger than the ones of the solid line(limestone layer) and the amplitude differences are

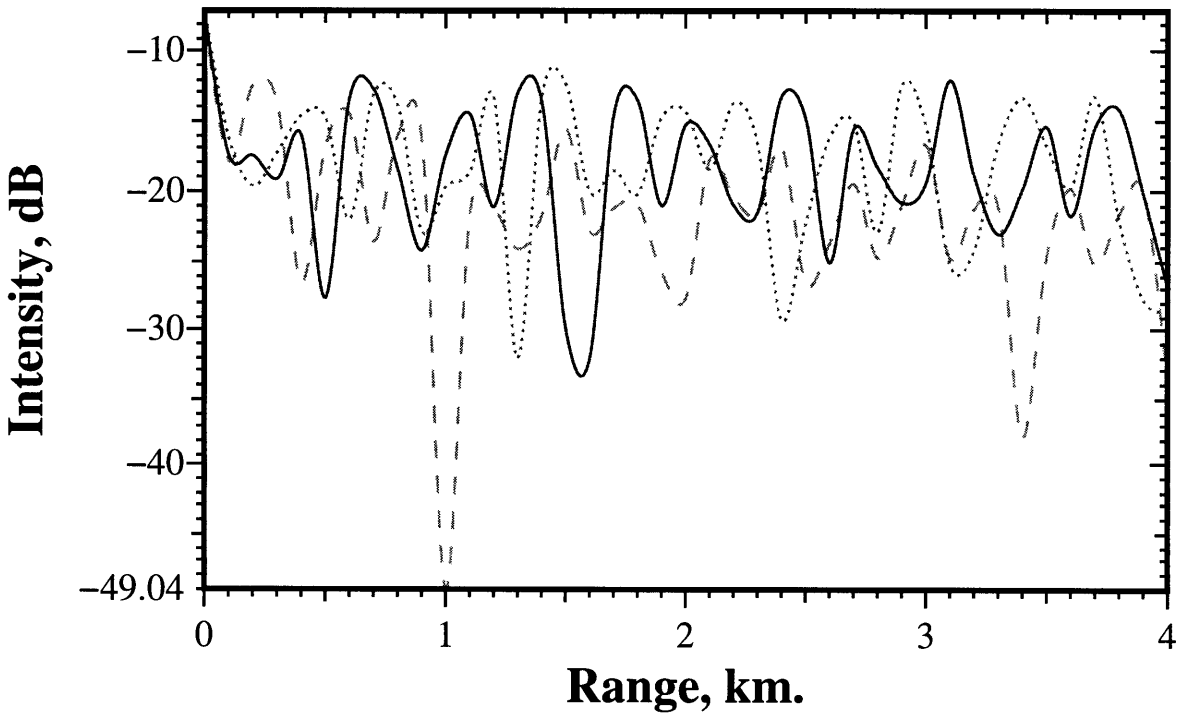

Figure 3-8: Mean fields for 3 types of the elastic layer over a basalt half space. The solid line is for limestone, the dashed line is for chalk, and the dotted line is for moraine.

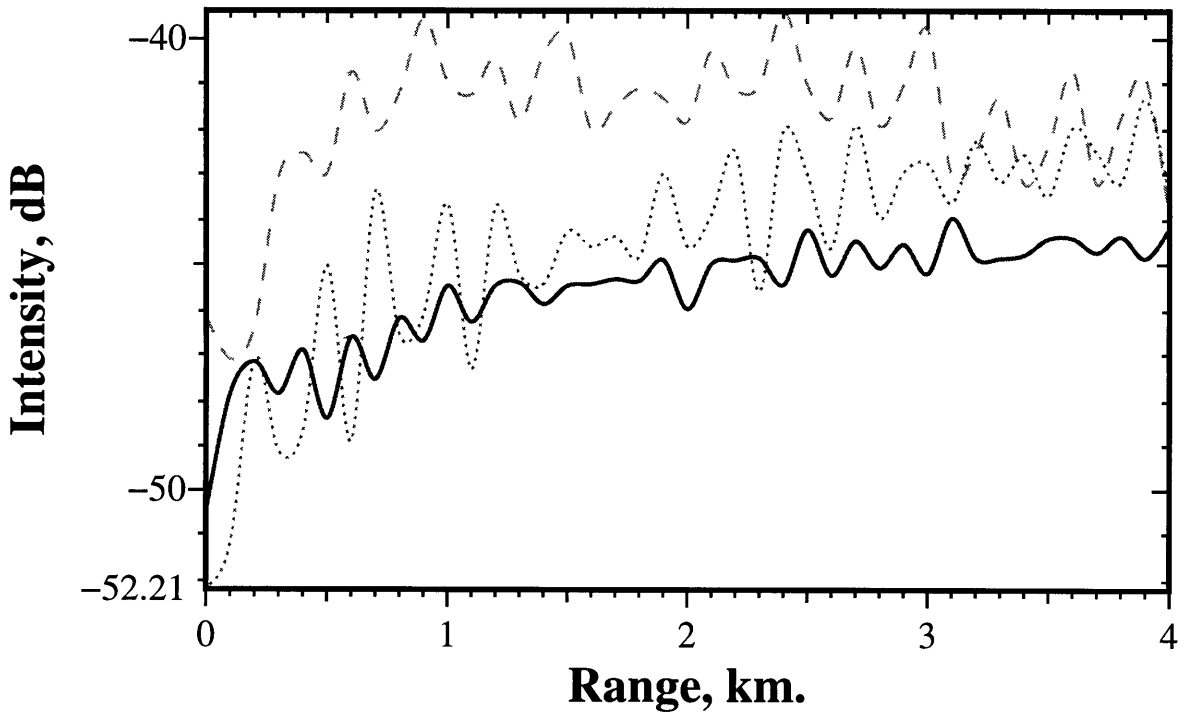

Figure 3-9: Scattered fields for 3 types of elastic layer over a basalt half space. The solid line is for limestone, the dashed line is for chalk, and the dotted line is for moraine.

bigger at long ranges. For the chalk layer, the mean field intensity is the smallest compared with the other two types but the scattered field is the biggest. The mean fields are similar at 1 km range but the differences increase with range. The range dependence of the scattered field is reverse. These differences between the mean and the scattered field are because the scattered field is a function of the mean field and its derivative at the rough surface, and the discontinuities in the scattered field and its derivative at the rough surface as shown in Eq. 2.34.

We can conclude that the scattered field is affected by bottom properties significantly and the patterns of changes in the mean and the scattered fields are quite different. If we compare the mean and scattered fields together, we might be able to get more information about the elastic layer in the bottom.

3.5 Modal Studies

Now we can study the scattered field using modes to understand the physics more easily and clearly. Although it is hard in practice to excite only one propagating mode in a shallow water waveguide, some scientists have studied how to excite s single mode and how this mode couples with other modes after excitation[7][28]. The single mode excitation gives us good insight about the mechanics of the scattered field.

Fig. 3-10 shows the scattered power vs. mode number and range for the 30 m thick limestone over a basalt half space. All the proper modes except the Scholte wave(mode 1) excite mode 6 strongly as shown in the upper picture in Fig. 3-10. This tells that all proper modes transfer energy to mode 6 by mode coupling. This is the same results as was observed due to thickness variations earlier in this chapter in Fig. 3-6. But incident mode 7, which is the last proper mode, excites the 7th mode but decays so quickly that it does not influence the scattered field at long range. When incident mode 6 is excited, it excites not only mode 6 itself but also mode 5 strongly. This means that two modes are coupled and energy is exchanged between two modes. All analyses by mode shapes and single mode excitation

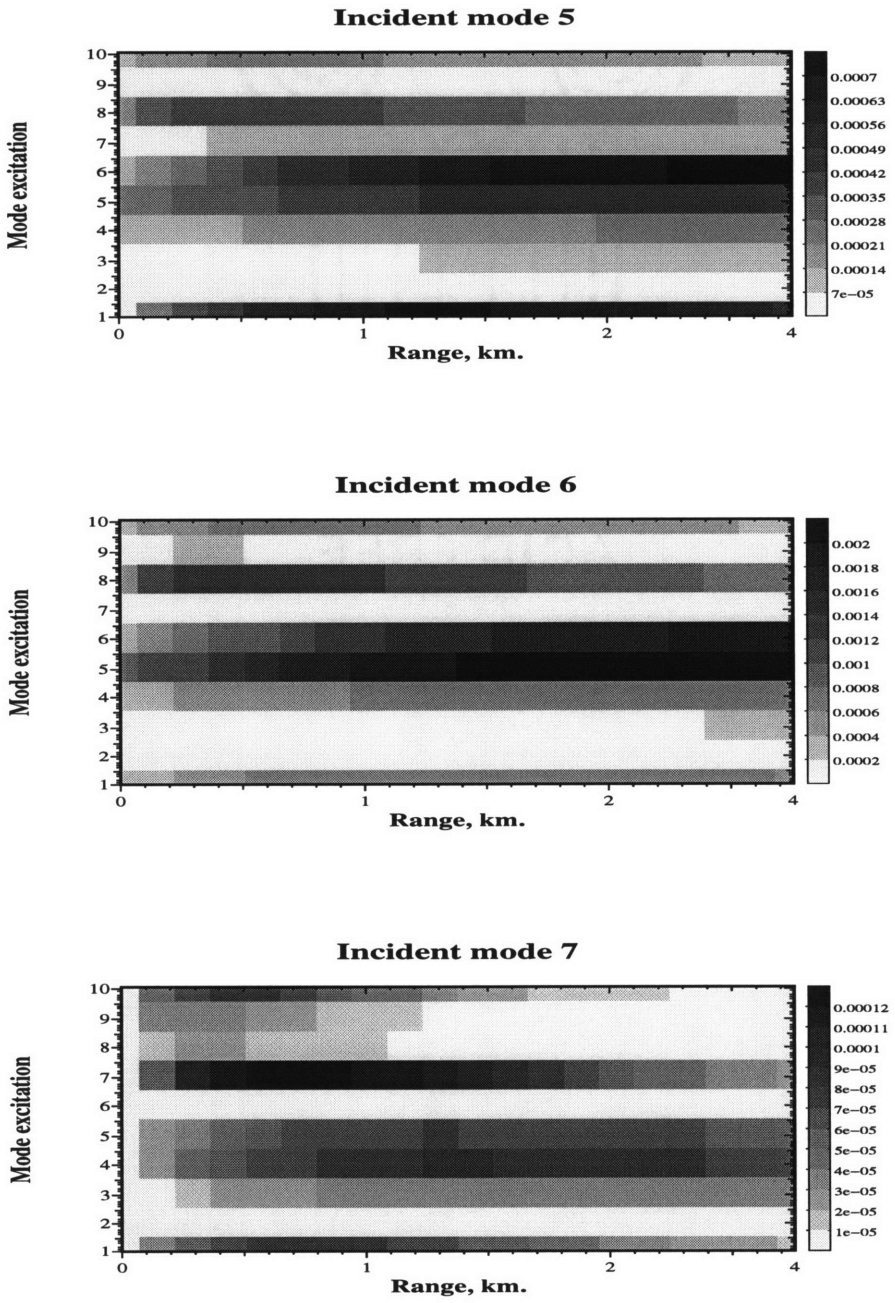

Figure 3-10: Single mode excitation for mode 5, 6 and 7. The colors show the scattered power vs. mode and range. 30m thick limestone over a basalt half space.

show consistent explanation of resonance of mode 6 which drives the scattered field strongly.

There is another useful way to look at the scattered field by modal statistics. Fig. 3-11 shows the cross-modal coherence at 0.5 km, 4 km, and 50 km for the 30 m limestone layer over a basalt half space. The left pictures are the normalized total field cross-modal coherence and the right ones are normalized forward-scattering field cross-modal coherence. At 0.5 km, all modes are highly coherent for the total field because forward propagating scattering is not significantly yet. For the scattered field, modal coherence is much less than the total field even at short ranges. At 4 km, only proper modes are highly coherent. The higher modes of the mean field are stripped, which means that the scattered modes dominate incoherent. The 1st mode is Scholte wave so it dies quickly to be incoherent. Mode 3 is incoherent even though this is a proper mode while the 2nd mode is highly coherent with other modes both in total and scattered field. Modes 5 and 6 in the scattered field show a little higher coherence because of modal energy transfer by coupling as was shown in Fig. 3-10. At long range(50 km), all modes are almost totally incoherent both in total and scattered field. This means that the scattered fields become dominant in the total fields at this range. The cross-modal coherence is a function of range so we can determine at a given range whether or not cross-modal coherence and the attribution of the scattered field are important.

These two modal studies could explain the scattering mechanisms. These studies could also be applied to a real experiment involving single mode excitation and data processing such as matched-field processing(MFP) and matched-mode processing(MMP) for cross-modal coherences[41].

3.6 Other Parameter Studies

Here we study some physics which are important or interesting in the scattered field in addition to the bottom properties and thickness. The parameters such as correlation length, the sound speed profile of water are studied with the effects of leaky modes, the forward and

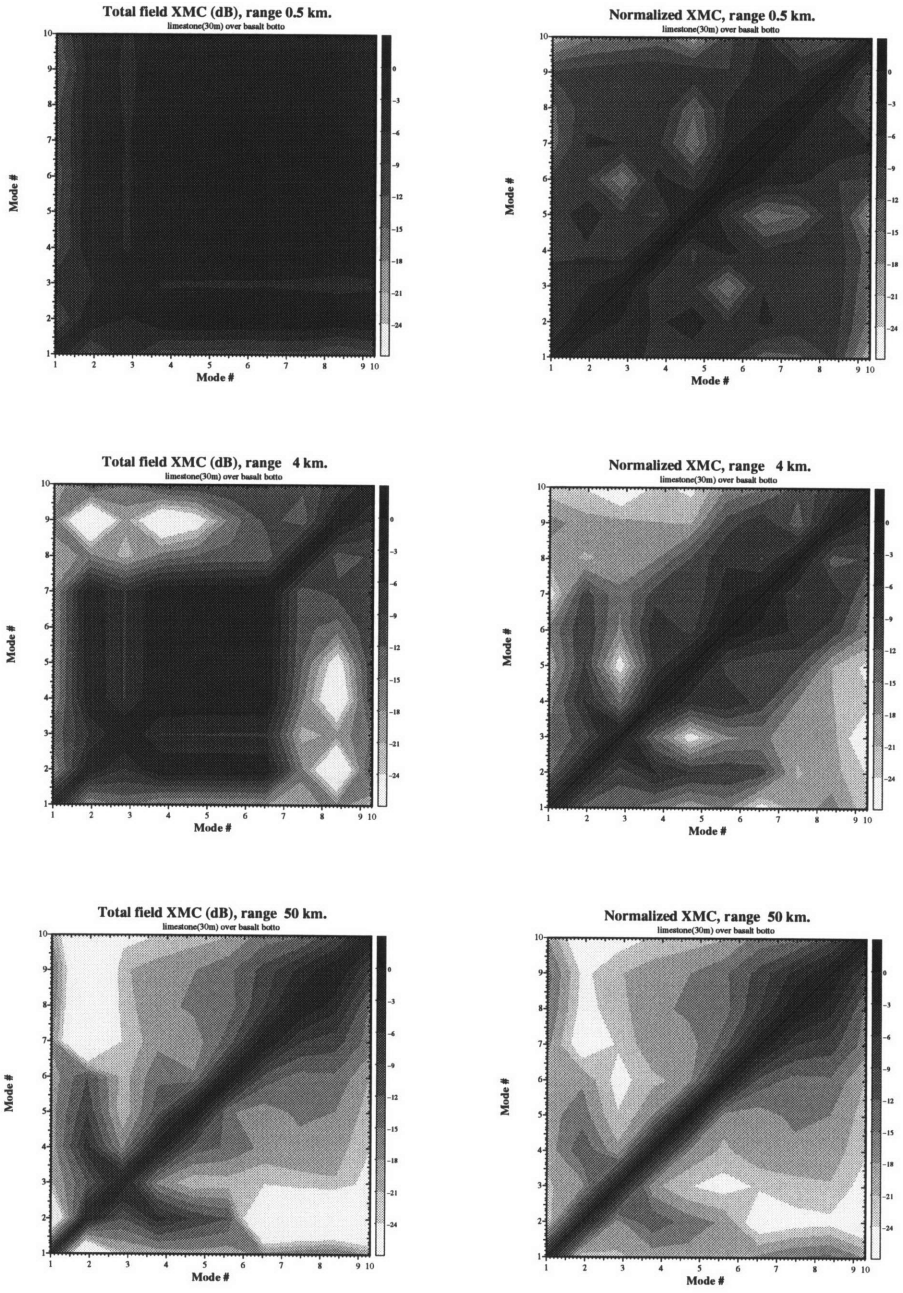

Figure 3-11: Cross-modal coherences(XMC) of the normalized total and scattered field for limestone(30m)-basalt half space bottom.

backward scattering contributions, the K/S self-consistent theory vs. the Born approximation in this section.

We mentioned the importance of modeling of the continuous spectrum. In order to see the importance of the leaky modes involved in computing the scattered field, we compare the scattered field calculated with and without leaky modes. In Fig. 3-12, the solid lines are calculated with all modes and the dashed lines represent the field computation without the leaky modes. The thickness of the limestone elastic layer is 30 m in this figure. At short range, the effect of the leaky modes is strong both in the mean field and the scattered field because the leaky modes are not attenuated yet. But at long ranges the leaky modes do not affect the scattered field significantly and the total field is mainly determined by the discrete spectrum. The leaky modes seem to have an important role in the scattered field relatively compared with the mean field though it is not distinct.

Next, we will show the effects of correlation length on the scattered field. The forward scattering becomes strong as the correlation length becomes large. We can easily see these effects in Fig. 3-13. The forward scattered fields (thin lines) do not vary significantly between three different correlation lengths while the backward scattering(thick lines) is more sensitive to the correlation length. When the correlation length is small compared to one wavelength(30 m), the forward scattering and backward scattering is of the same order of magnitude(seen in the two solid lines). When the correlation length is large compared with one wavelength, the forward scattering is much bigger than the backward scattering(seen in dotted lines). The longer correlation length scatters most of the energy to the specular direction because each section of rough surface acts like an array of coherent virtual sources which are added in coherently over the surface length. The short correlation length spread the scattered energy to large wavenumbers because the rough surface acts like a collection of random diffractions.

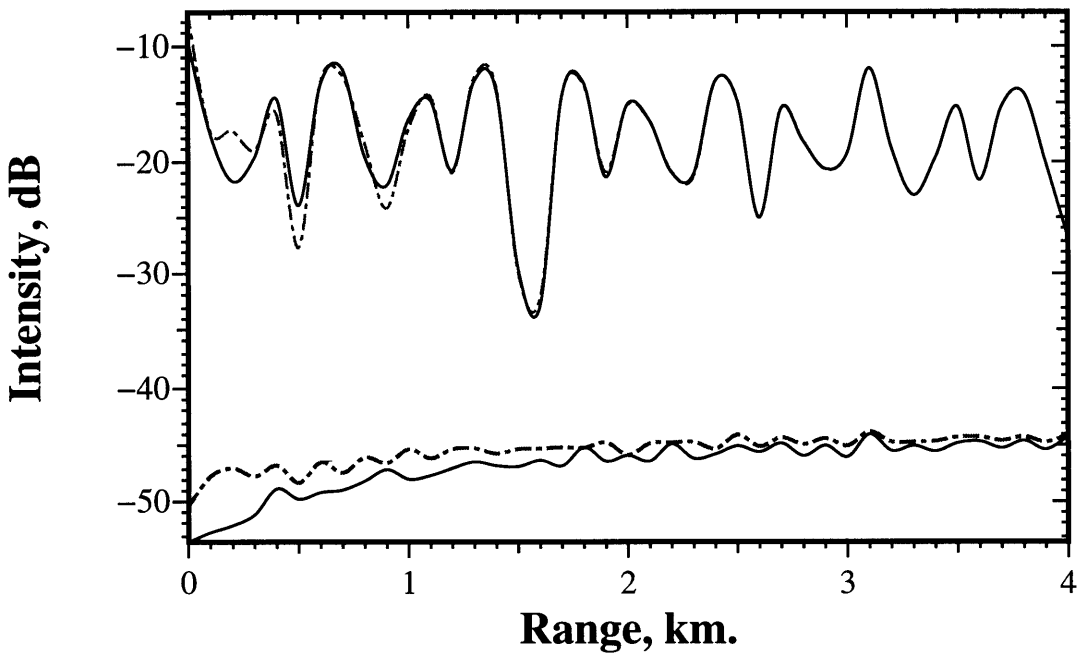

Figure 3-12: Leaky mode effects on the mean fields and the scattered fields from all modes and proper modes only. The solid lines are for proper modes and the dashed lines are for all modes. The top two curves are the mean fields and the lower two curves are the scattered fields in case of 30 m limestone layer over a basalt half space

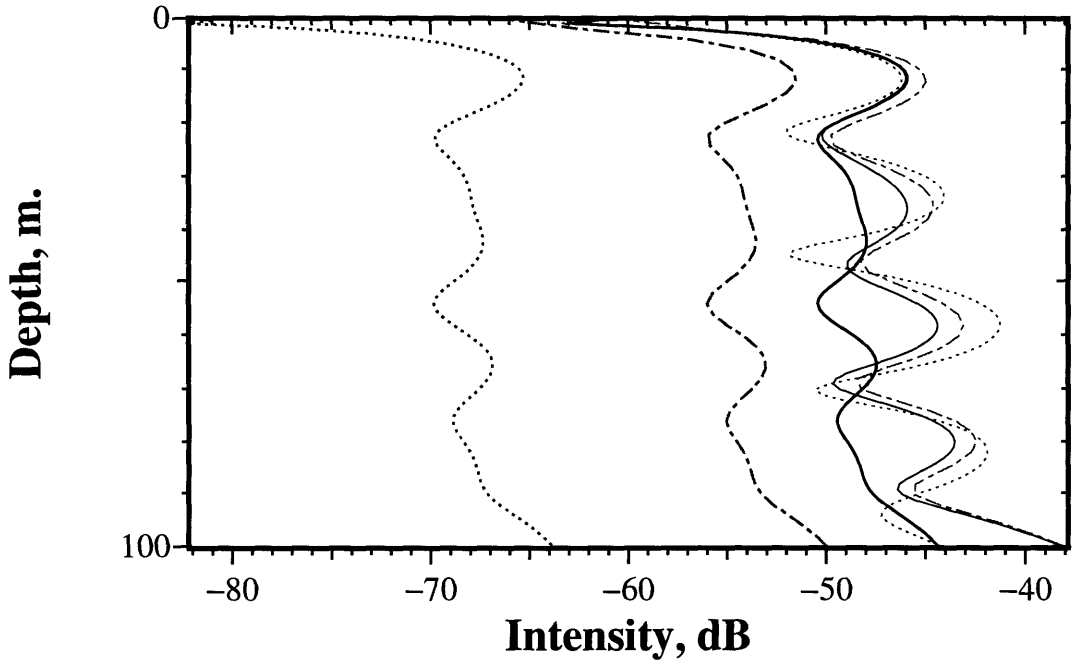

Figure 3-13: Effect of correlation lengths. The thick lines are the backward scattering and the thin lines are the forward scattering at 4 km range. The solid lines are for CL=10 m, the dashed lines are for CL=20 m, and the dotted lines are for CL=100 m. The RMS height is 1 m.

Next we analyze how much the forward and backward scattering affect the total field as a function of range. In Fig. 3-14, the forward scattering converges to the total field at long range because backscattering becomes smaller at long range. But at short range, backscattering is bigger than or comparable to the forward scattering.

Now we examine the effect of the sound speed profile(SSP) on the scattered field. For a downward refracting SSP, the scattered field intensity is known to be high because the waves interact a lot with bottom. This is shown in Fig. 3-15 using thin curves, where a 10 m limestone layer over a basalt half space was used. The thin solid line is the expected scattered field from an iso-velocity profile and the dotted line is from the downward refracting profile. The expected scattered field intensity is 2 – 3 dB bigger for the realistic downward refracting profile as we expected. However, for the 30 m limestone layer case, the downward refracting sound speed profile(thick solid line) gives a small scattered field intensity compared with the isovelocity profile(thick dashed line). The reason is thought that the scattered field is driven by resonant mode 6 for the isovelocity SSP but mode 6 is somewhat away from resonance when the downward refracting profile is used to calculate the scattered field. Scattering is quite a complicated phenomenon which involves many parameters and physics of environment.

For computational reasons, we have used the Born approximation so far to calculate the scattered field but we developed the self-consistent theory in Chapter 2. We can apply the self-consistent theory to calculate the scattered field by using both OASES and KRAKEN to consider modal scattering loss in the mean field. The mean field from self-consistent calculations become smaller than the one from the Born approximation because of the scattering loss in the mean field. This is shown in the mean fields in Fig. 3-16. The mean and the scattered fields from self-consistent theory give smaller intensities because the mean field includes the scattering losses. But for this one limestone layer scenario, the effects of fast decay or growing in the scattered field are not distinct as shown in Tracey's thesis [40].

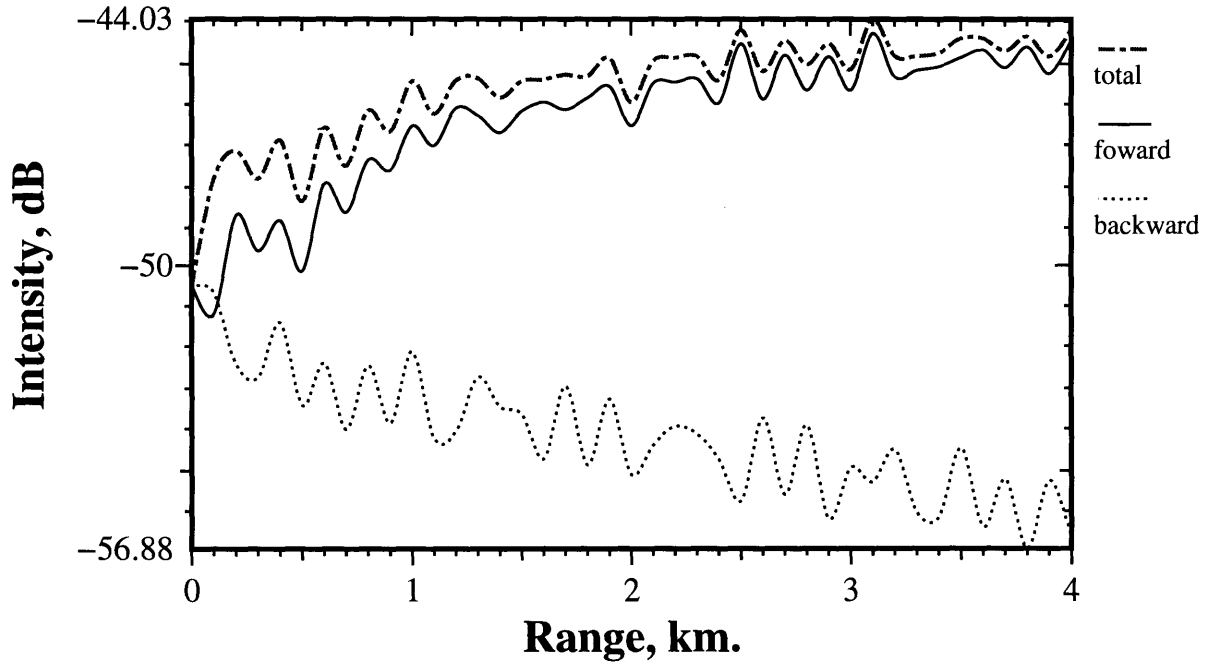

Figure 3-14: Contribution of the forward and backward scattering to the total scattered field. The solid line is the forward scattering, the dotted line is backward scattering, and the dashed line is the total field

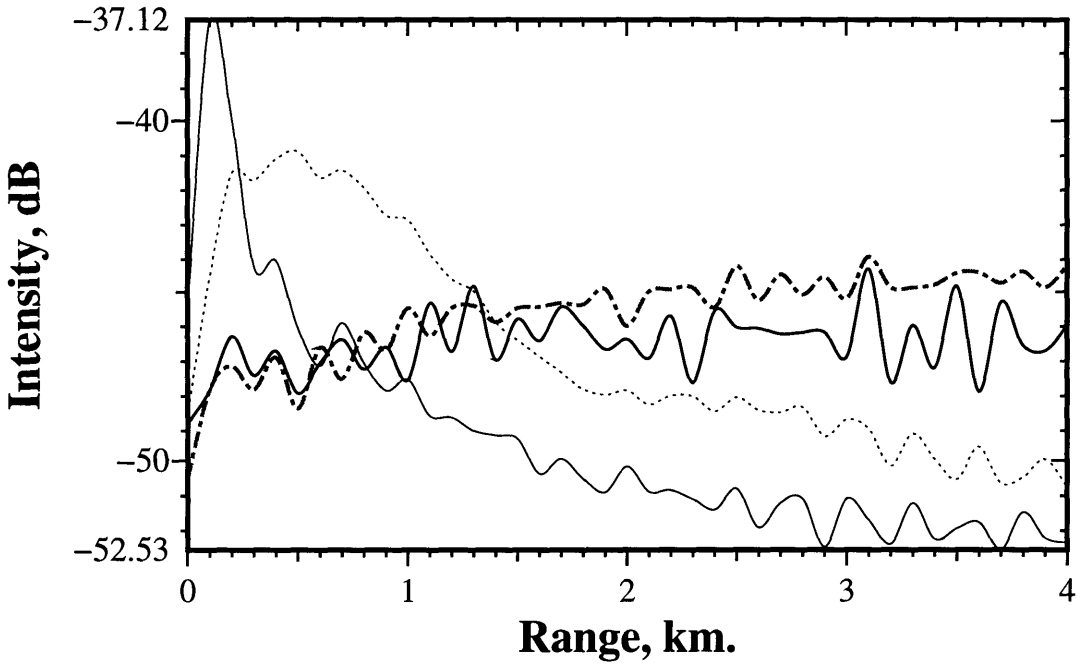

Figure 3-15: Effect of sound speed profile of water column on the scattered field intensity. The thick lines are for 30m limestone layer over a basalt half space. The thin lines are for 20 m layer. The thin solid line and the thick dashed line are from isovelocity sound speed profile(SSP), the thick solid line and the thin dotted line are from downward refracting SSP(linear slope from 1500 m/s for top to 1480 m/s for bottom).

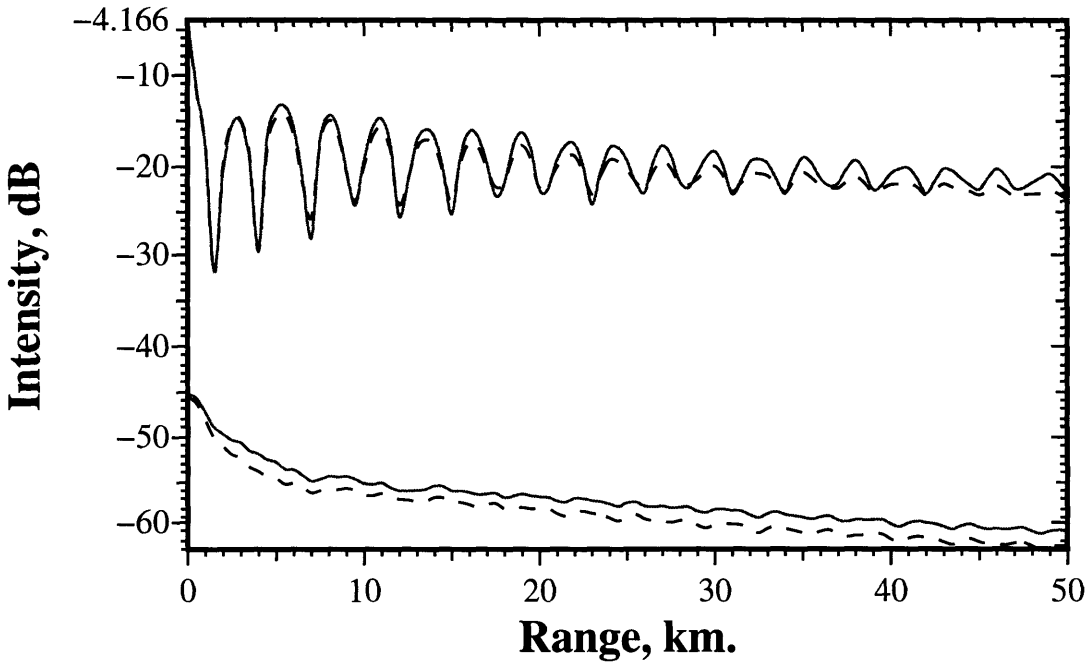

Figure 3-16: Mean and scattered field intensities from self-consistent and Born approximation calculations. The solid lines are Born approximation and the dashed lines are self-consistent theory. The upper two lines are the mean fields and the two lower lines are the scattered fields.

3.7 Summary

In this chapter, we apply the theory developed in Chapter 2 to study scattering. The extended NMSCAT code was used to calculate the scattered field considering one elastic layer over a half space. The comparison with OASS shows good agreement and validates this theory and code to study scattering. The inclusion of one elastic layer over a half space can compute more realistic scattered fields compared with the half space model. This tells the importance of a layered bottom model for the scattered field. The thickness and different bottom types of the elastic layer also affect the scattered field significantly. The scattered field is more sensitive to change in the depth and properties of the elastic layer. If we study the scattered field with the mean field, we might get more information about these parameters in the bottom. Using modal analysis, we showed that the modal approach is very good way to study scattering mechanisms. Other parameter studies which affect the scattered field were also shown in this chapter.

However, the real ocean bottom has many layers. The inclusion of more layers in the model is required to predict the scattered field more accurately. We will pursue the study of the effects of multiple layers in the next chapter.

Chapter 4

Scattering Considering Multiple Layers in the Bottom

In chapter 3, we showed that one elastic layer could affect the scattered field significantly. The inclusion of one elastic layer can yield more realistic results compared with the half space case. However the structure of the real ocean bottom has many elastic layers. Moreover, all interfaces in the real bottom have roughness. It is hard to consider all the rough interfaces and elastic layers in a numerical model. In order to consider many rough surfaces, we need to consider multiple scattering. The multiple scattering phenomena are not clearly understood yet and can be neglected in many cases or can be estimated by the single scattering problem because the problem of multiple scattering of waves is a kind of a linear version of the many-body problem[4]. Here we also neglect the multiple scattering which means that only one interface has roughness. We developed the theory to consider any rough surface in the bottom, but here we assume only fluid-elastic interface has roughness because the modal code to calculate the mean field in the elastic layers are not available now.

We have used some more assumptions and restrictions to model the bottom as multiple layers. In the following section, we will discuss those assumptions and restrictions. The scattered fields from the multiple layered model is compared with the reference solution

from OASS. Then we will simulate the scattered field with the geoacoustic bottom data from the Korea Strait experiment.

4.1 Modeling of Scattering from Multiple Layers

4.1.1 Assumptions and Restrictions

In addition to the general assumptions of horizontally stratification and range independence, we have to use another assumption in calculating the expected scattered fields in the water column for the case of multiple elastic layers. We calculate the scattered field only in the water column, which is the field of significance to sonar systems.

We need to use the mean fields as a source of the scattered field as in Eq. 2.46. Unfortunately, the normal mode code KRAKENC cannot calculate the displacement and stress amplitudes of the mean field in arbitrary elastic layers. Therefore we obtain the mean fields by solving the boundary matrix equation as stated in Chapter 2. We used the standard matrix solver to compute this matrix equation but the solver becomes unstable when many layers are considered. The Direct Global Matrix solver[19] can make the solution stable even when many layers are considered.

If a modal code to compute the displacement and stress in the elastic layers were available, we can compute the mean fields and replace them in the right hand side of Eq. 2.46. Then we can compute the scattered field correctly. We can also get rid of the restriction that only the fluid-elastic layer has roughness. We can easily modify the NMSCAT code to calculate the scattered field in the water column from any rough interface in the elastic layers. Moreover, we can calculate the scattered fields in the elastic layers. If we get the scattered field by using the impedance boundary conditions in Eq. 2.48, we also can replace that field in the water in Eq. 2.47 and solve the matrix. Then we can get the scattered fields in all elastic layers.

Since this advanced modal code was not available at the initial stage of this work, we

assume that the components of the mean fields as computed by the current modal code are the same whether we consider many elastic layers or one elastic layer over a half space. This assumption is unjustified when the first layer is very thin and the attenuation is small. However, when the loss in the first or second layer is large enough, the assumption is valid, because the differences come from up and downward components of the waves in the second elastic layer and these errors should be very small.

Therefore we can calculate the scattered field in the fluid reasonably well with the restrictions when the first or second elastic layer is quite thick or the attenuation of the 1st or 2nd layer is high enough not to affect the modal components of the up and down waves in the first layer. We show these in detail in the following sections.

4.1.2 Scattering from Two Layers Over a Half Space

In order to maintain consistency with the previous chapter, we put another elastic layer between the limestone and the basalt half space. The density of this elastic layer is 2.5 g/cm^3 and the compressional and shear wave speeds are 4000 m/s and 2000 m/s, respectively. The attenuation coefficients are assumed to be the same as in the limestone and the basalt.

Fig. 4-1 shows the scattered fields calculated by considering 2 elastic layers over a basalt half space. The first and the second layer thicknesses are 10 m in this calculation. The solid line is from NMSCAT and the dashed line is from OASS. The overall differences are about 5 dB between these two models but the overall pattern of two results is similar. The main source of error is thought to results from the incorrect calculation of the mean fields in the first elastic layer as we described in the previous section. If this is true, the results of the two models should become similar as the thickness of the first layer is increased, because the upgoing and downgoing components of the waves in the first layer are not greatly affected by layers below when the first layer is thick enough or attenuated highly.

In order to verify this, the thickness of the first elastic layer is changed to 30 m and that of the second layer is changed to 20 m. In Fig. 4-2, the differences between two models are

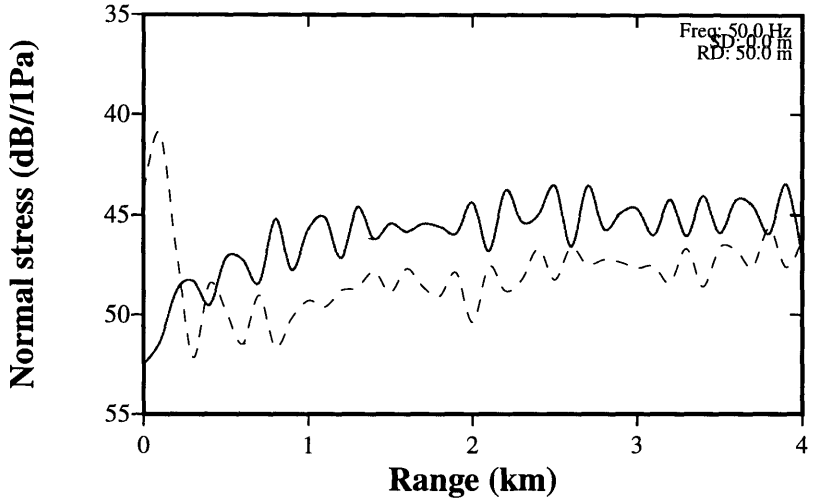

Figure 4-1: Comparison of the scattered fields from OASS and NMSCAT in the case of a bottom with 2 elastic layers over a half space. The thickness of each of the two layers is 10 m. The solid line is from NMSCAT and the dashed one is from OASS.

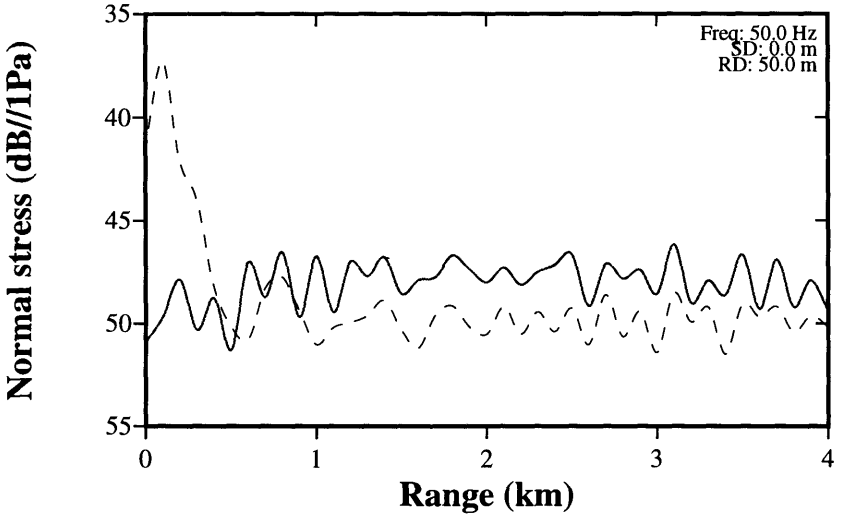

Figure 4-2: Comparison of the scattered field from OASS and NMSCAT. Properties are the same as in Fig. 4-1 except that the layer thicknesses are 30 m for the 1st and 20 m for the 2nd. The solid line is from NMSCAT and the dashed one is from OASS.

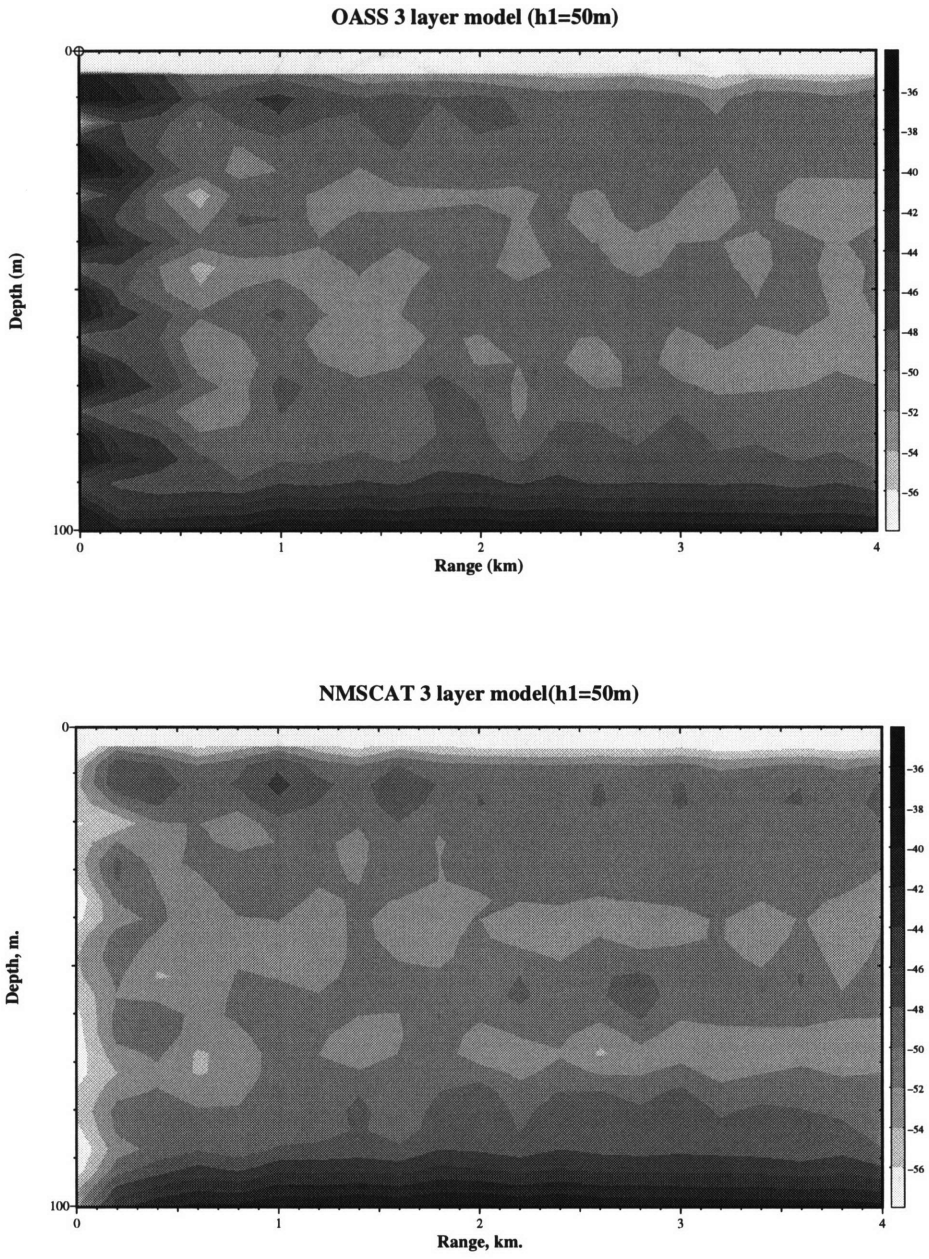

Figure 4-3: Comparison of the scattered field vs. range and depth from OASS and NMSCAT when the first and second layers are 50 m thick. The upper picture is from OASS and the lower one from NMSCAT.

smaller and the interference pattern looks similar. The differences are about 3 dB at all ranges. When the first limestone layer is 50 m thick, they are almost the same amplitude except at short range as shown in Fig. 4-3. These results confirm the hypothesis that errors in the computation of the mean field are responsible for the discrepancy between NMSCAT and OASS.

We can also examine the effects of the second layer. We changed the thickness of the second layer to 40 m while maintains the thickness of the first layer at 10 m. Fig. 4-4 shows good agreement of the two scattered fields in both amplitude and interference pattern except at short range. It also supports our hypothesis that the up and downgoing waves in the first layer are not affected by the second layer when the second layer acts like a half space. This fact tells us that we can use this code to calculate the scattered field in the fluid when the real bottom has a thick or high attenuated 1st or 2nd layer. We considered bottom types such as limestone and basalt which have low attenuation and high impedance. Realistic bottom types which are usually high attenuation and low impedance surely give more accurate scattered fields, because the mean field of the first layer is not affected significantly.

4.1.3 Scattering from Multiple Layers

Here, we add more elastic layers between the limestone and basalt as shown in Table 4.1. First, another elastic layer is put right above the basalt half space. The acoustic parameters of each layer are bounded by those of the basalt and limestone. All the layers over the basalt half space are 10 m thick each. As we expect, the scattered field is not error-free due to the incorrect mean field calculation as shown in Fig. 4-5. The error is in fact a little bigger than in Fig. 4-1. That is because the error of the mean field grows when more layers are considered. The error is about 5 dB range because up and downgoing waves in the first layer are mainly determined by the first two layers in this example. The error range seems to be almost the same when 4 layers are considered(Fig. 4-6). This is thought that the layers below the third layer do not affect the first layer.

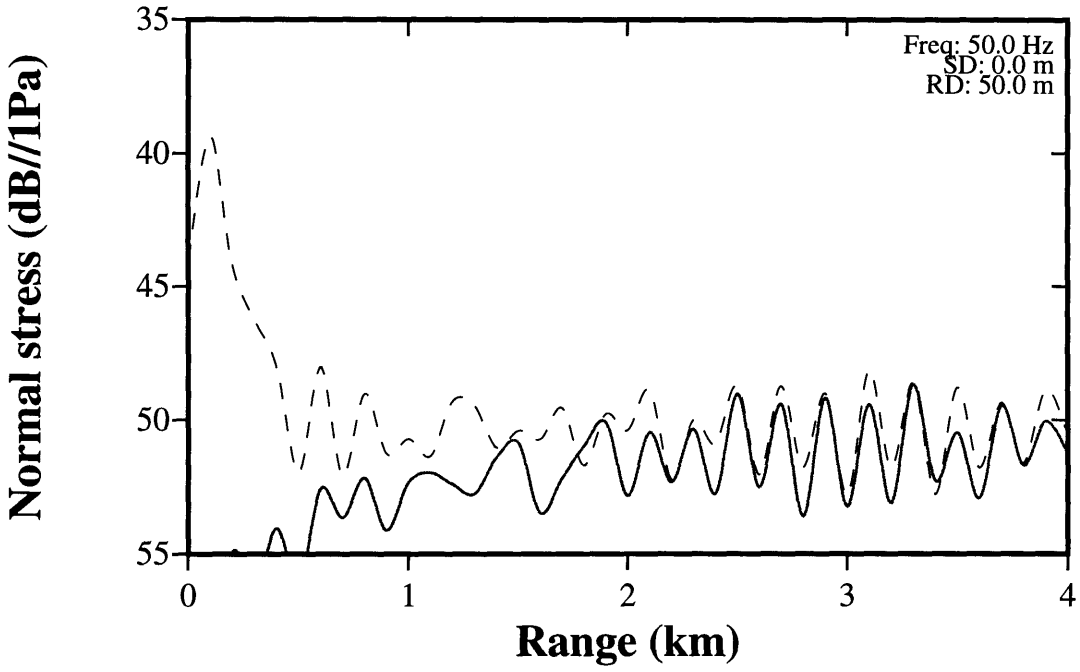

Figure 4-4: Comparison of the scattered fields from OASS and NMSCAT in the case of a bottom composed of 2 elastic layers over a basalt half space. The second layer is 40 m thick while the first layer is 10 m. The solid is from NMSCAT and the dashed line is from OASS.

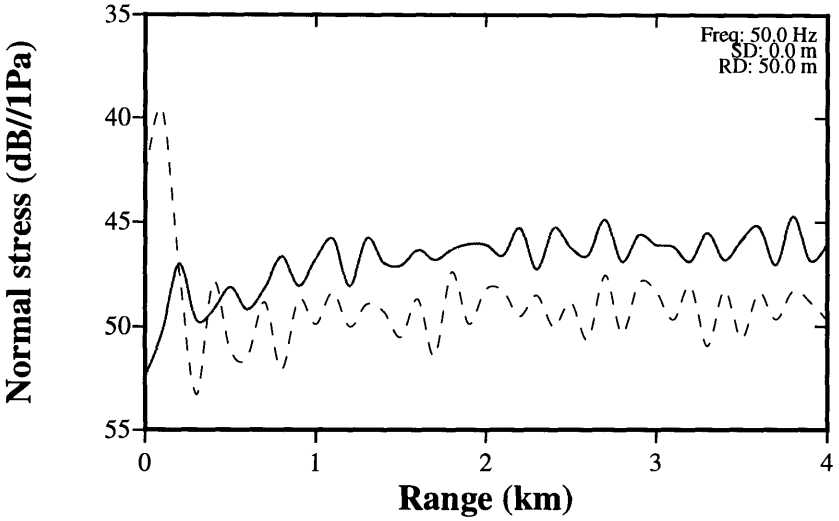

Figure 4-5: Comparison of the scattered fields from OASS and NMSCAT in the case of a bottom with 3 elastic layers(10 m thick) over a basalt half space. The solid line is from NMSCAT and the dashed one is from OASS.

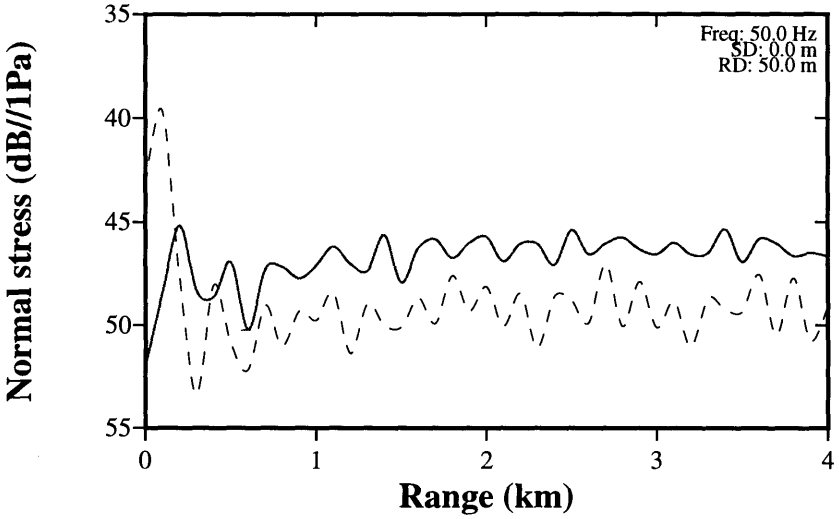

Figure 4-6: Comparison of the scattered fields from OASS and NMSCAT in the case of a bottom with 4 elastic layers(10 m thick) over a basalt half space. The solid line is from NMSCAT and the dashed one is from OASS.

Table 4.1: Geoacoustic properties of the 10 elastic layers to be used for multi-layered bottom.

No. of layer	*Density*(g/cm^3)	$c_p(m/s)$	$c_s(m/s)$
1(limestone)	2.40	3000	1700
2	2.45	3500	1800
3(2 layered model)	2.50	4000	2000
4	2.55	4250	2100
5(3 layered model)	2.60	4500	2200
6	2.62	4600	2250
7(4 layered model)	2.64	4700	2300
8	2.66	4800	2350
9	2.68	4900	2400
10(basalt)	2.70	4250	2500

As the thickness of the first elastic layer is increased, the results from OASS and NMSCAT are almost the same as a function of depth and range(Figs. 4-7 and 4-8). We can see a little big difference in this case compared with Fig. 4-3 because of the bigger error of the mean field components.

The trend continues in the case of 10 layers. The properties are shown in Table 4.1. In Fig. 4.9, the interference patterns are almost the same except at short range while amplitude differences exist.

It is interesting to observe the scattered fields as a function of the number of layers. Although we cannot find any consistent pattern of change, the scattered fields are distinct for each number of elastic layers. We can conclude that the scattered field can be predicted more realistically when the bottom is modeled as multiple layers.

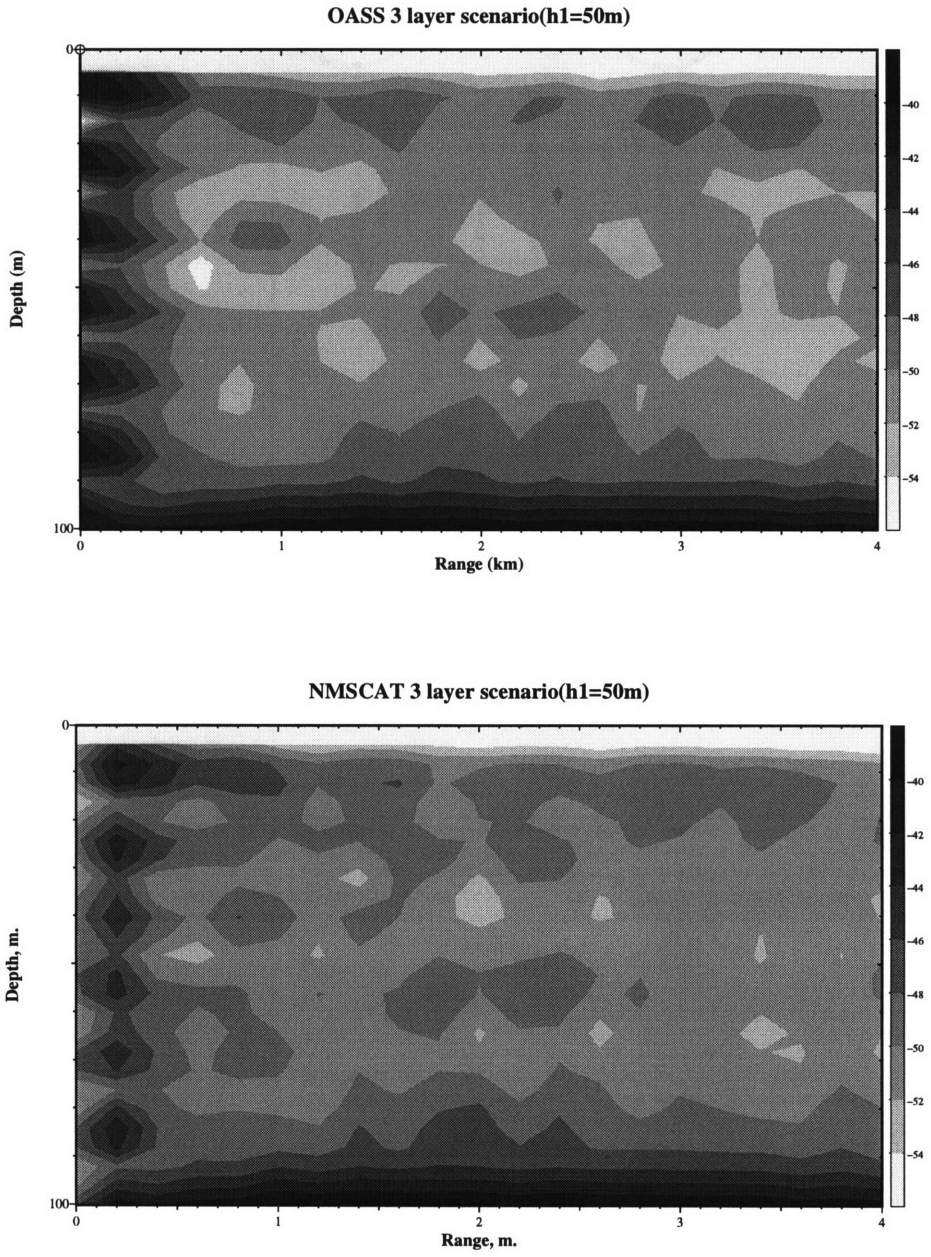

Figure 4-7: Comparison of the scattered fields from OASS and NMSCAT vs. depth and range in the case of a bottom with 3 elastic layers with 50 m thickness for the first layer. The upper picture is from NMSCAT and the lower one is from OASS.

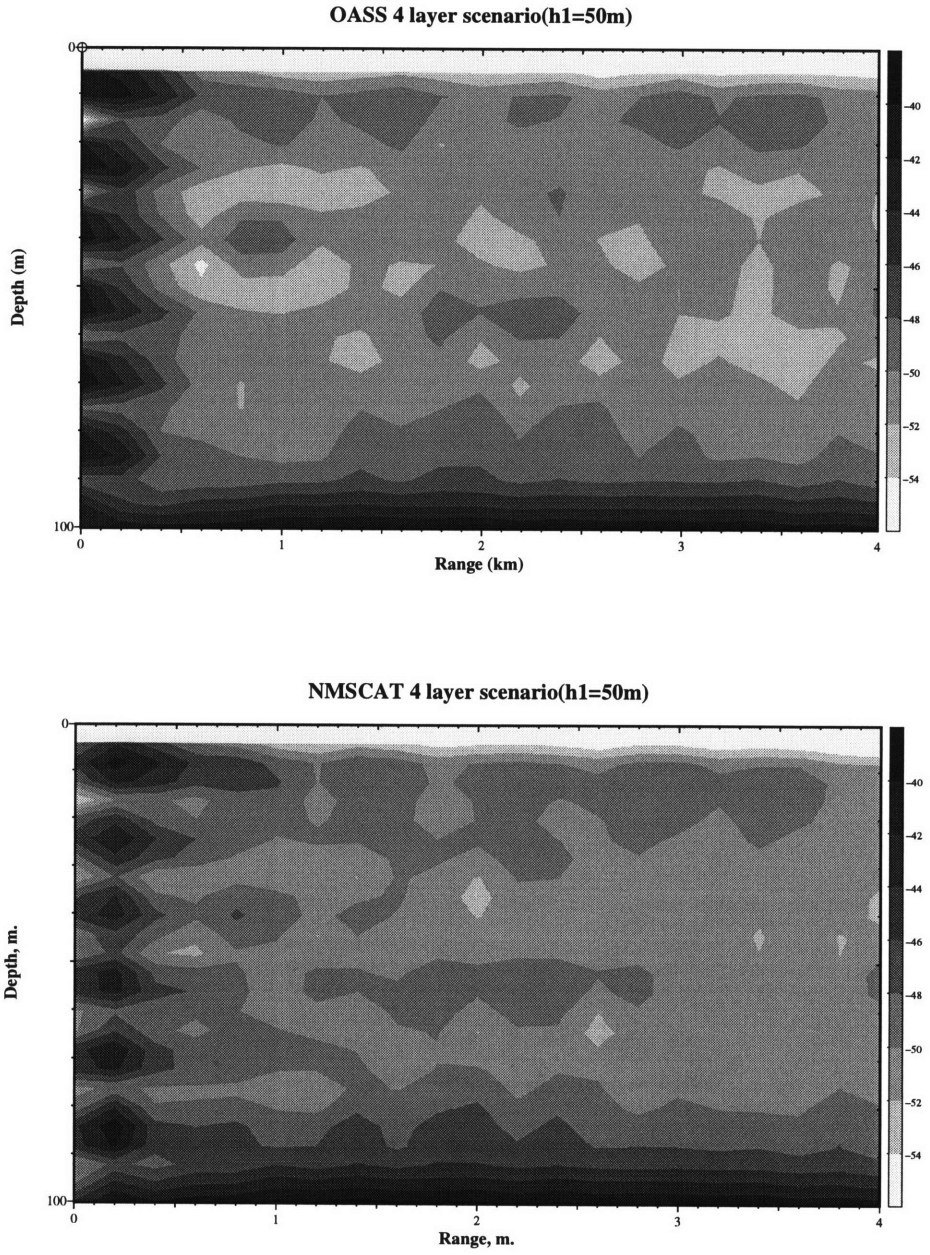

Figure 4-8: Comparison of the scattered fields from OASS and NMSCAT in the case of a bottom with 4 elastic layers with 50 m thickness for the first layer. The upper picture is from NMSCAT and the lower one is from OASS.

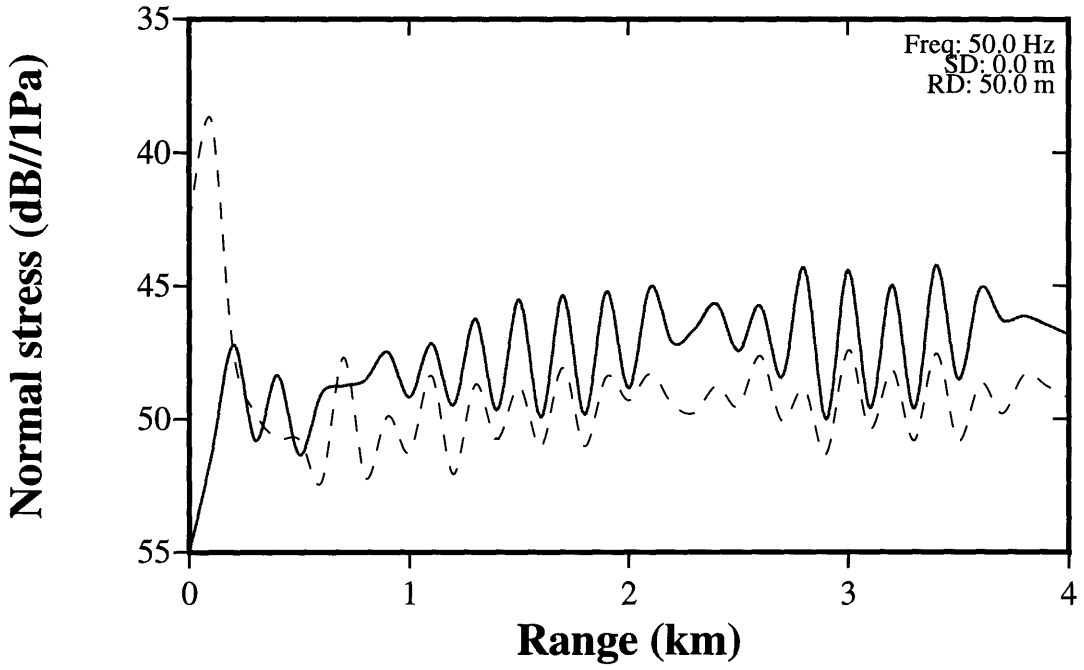

Figure 4-9: Comparison of the scattered fields from OASS and NMSCAT in the case of a bottom with 9 elastic layers (10 m for each) over a basalt half space. The solid line is from NMSCAT and the dashed one is from OASS.

4.2 Simulation of the Scattered Field in the Korean Experiment

Up to now, we have dealt with unrealistic hard bottoms to aid in understanding the scattering physics. Usual shallow water bottoms are composed of unconsolidated sediments such as clay, silt or sand for the first layer and moraine or chalk for the basement. We will study scattering in the Strait of Korea using measured bottom properties.

The ACT III(The Third Acoustic Characterization Test) was performed in the Strait of Korea in summer in 1995. The Strait of Korea is a typical shallow water environment; it is very complicated, with strong tides, currents, the fronts, and internal waves. During this experiment, geoacoustic data of the bottom were collected by the grab samples and 3.5 kHz precision depth recorder data and the Japanese seismic lines. After analysis of all historical and experimental data, Lynch *et al.*[24] suggest that the bottom can be modeled as three layers including a moraine half space as seen in Fig. 4-10. For the bottom statistics of RMS height and correlation length, we choose the same values as in the previous chapter because they are not stated in Ref. [22]. The RMS height and the correlation length are quite important to know exactly but they are not variable for one experiment site. We will examine layer effects of the bottom to affect the scattered field because others already study the effects of rough statistics numerically[41][23]. There are two main parameter's to be examined: one is the thickness of the first layer(10 – 20 m)[24] and the other is the wave velocity of the second layer(1760 $\pm$ 80 m/s). We will study how these uncertainties affect the scattered field. First, we need to show that NMSCAT is an appropriate model for this.

NMSCAT is believed to be adequate to calculate the scattered field with two layers over a moraine half space because the attenuation in the first layer is quite high and the second layer is quite thick. In order to make sure, the scattered field calculated by NMSCAT is compared with one by OASS. Fig. 4-11 shows the results from NMSCAT and OASS. Although there is a 2 dB difference, NMSCAT is quite good model to study the scattering in the Korea Strait experiment because the error lie within 2 dB of each other which is acceptably low and the

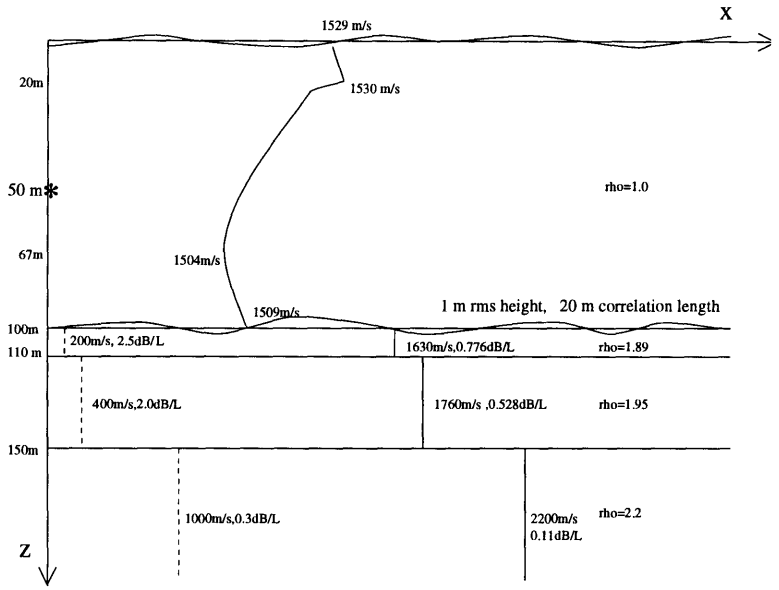

Figure 4-10: ACT III-the Korea Strait experiment scenario. L is the wave length in this scenario.

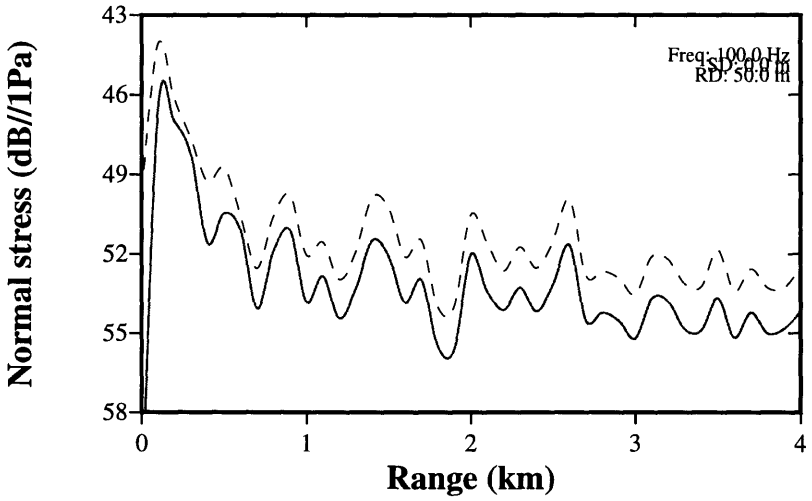

Figure 4-11: Comparison of the scattered field from NMSCAT and OASS with Korea Strait experimental geoacoustical bottom data. The solid line is from NMSCAT and the dashed line from OASS.

interference patterns are exactly the same over all ranges.

First, we will find how the thickness of the first shelly silty sand layer affects the scattered field. From the two curves in the lower part in Fig. 4-12, we can see a difference of more than 2 dB at long ranges while relatively good agreement exists at short ranges. The scattered field from 10 m shelly silty sand layered bottom is 2–3 dB higher than in the 20 m case at long ranges. This is exactly what we expect because the higher attenuation of scattered waves in the first layer. The interference patterns are similar although they are not identical. It is very interesting to look at the difference in the mean fields of the two models, which is small at short ranges but increases with range. The overall amplitude is the same but only the amplitude of the wiggly components are somewhat different. It is quite different feature from the scattered fields. We can observe that the thickness of the first layer affects the mean and scattered fields in different ways. This suggests that if we study the mean and scattered fields together, we may get more information about the thickness of the first elastic layer although it is not easy to determine the thickness of each layer at this stage.

The geoacoustic parameters for the first elastic layer are usually known in the shallow water by grab samples and other direct or indirect measurements. The basement subbottom properties are also identified by historical data and acoustical measurements. On the other hand, the properties of the second or the other layers may not be available in many cases. We can research the effect of the second elastic layer in the Korea Strait experiment.

We assume that we know the thickness and acoustic parameters of the first elastic layer but are unsure about the second layer. In order to remove the attenuation effects, the same attenuation coefficients are used for the second layer. The density and compressional and shear speeds of the second layer are set to 2.00 g/cm^3, 1788 m/s, and 600 m/s, respectively. The results are shown in Fig. 4-13.

The scattered field from the new second layer is 3 dB or more higher than the original scenario over all ranges. The harder bottom yields more intense scattering as expected. We cannot see much effects of the harder bottom in the mean field, Rather the mean field from

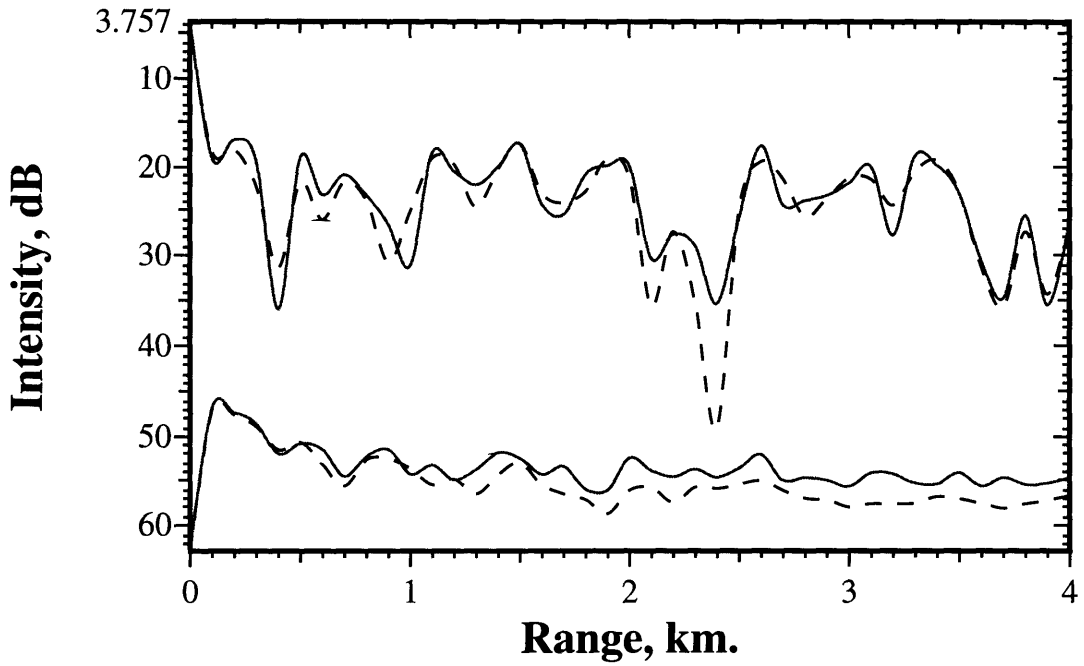

Figure 4-12: Effect of thickness of the first shelly silty sand layer on the mean and scattered fields. The upper two curves are the mean fields and the lower two curves are the scattered fields. The solid lines are for 10 m thickness and the dashed ones are for 20 m thickness.

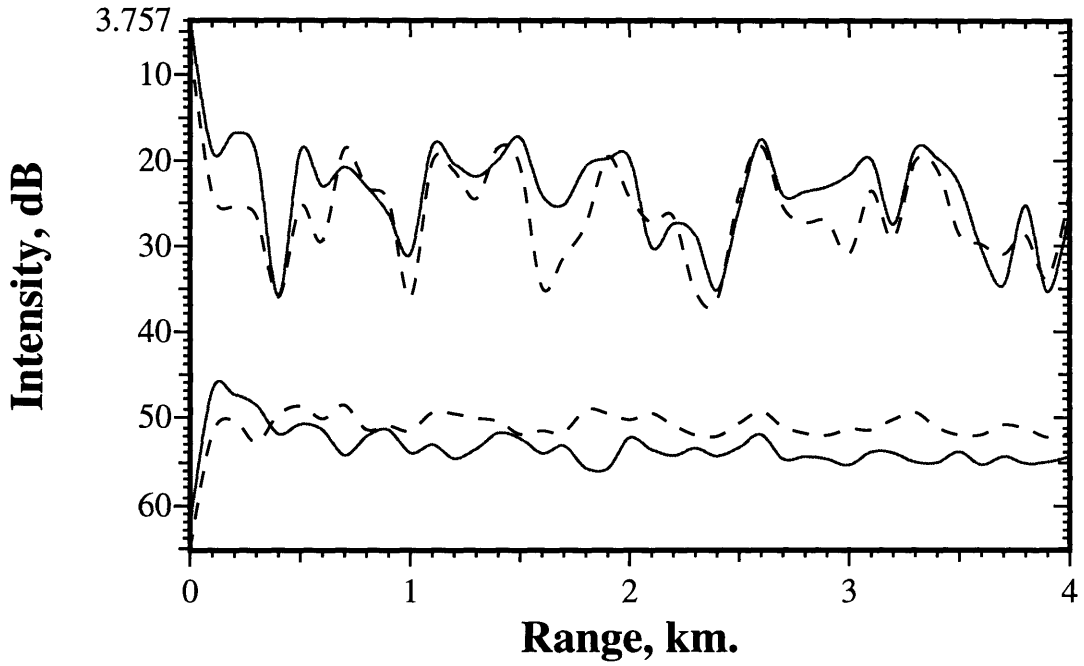

Figure 4-13: Effect of the elastic properties of the second layer on the mean and the scattered fields. The upper two curves are the mean fields and the lower two curves are the scattered fields. The dashed line is for a new second layer while the solid one is for the Korea Strait scenario. $\rho = 2.0 g/cm^3$, $c_p = 1788 m/s$, $c_s = 600 m/s$ for new second layer while $\rho = 1.95 g/cm^3$, $c_p = 1760 m/s$, $c_s = 400 m/s$ for the Korea Strait scenario.

harder bottom is slightly smaller. The interference patterns are quite different between two models, both for the mean and scattered fields. The different material in the second layer affects the mean and the scattered fields significantly.

We can see these differences at all depths and ranges in Fig. 4-14. The two pictures at the top of Fig. 4-14 show thickness effects. The amplitude and the interference pattern at short range are almost the same. As the range increases, the scattered intensities from the 20 m thick layer become 2 dB smaller or more. In the lower picture, we can see the strong modal features at all depths and ranges. The intensities are 2–4 dB higher than in the original Korea Strait scenario. We expect the scattered field in this case to be strongly driven by one or two modes as we discussed it in Chapter 3. We now examine these modal shapes.

For the Korea Strait scenario, we get 6 proper modes out of 20 modes calculated by KRAKENC. The first mode is the Scholte wave whose phase speed is lower than the fluid. We get 19 modes for a 20 m 1st layer scenario and 16 modes for a new 2nd layer scenario. Both have 6 proper modes and one Scholte wave mode. We show only 10 modes in Fig. 4-15. The proper modes from 2 to 6 mode are almost the same but the last proper mode 7 and the three leaky modes are quite different as shown in Fig. 4-15. If we observe the bottom pictures(a new 2nd layer) of Figs. 4-14 and 4-15, we can easily notice that the pattern of the scattered field is similar to the 8th mode shape, the first leaky mode. This means that the scattered field is strongly driven by mode 8 in this scenario.

For the middle picture(20 m 1st layer) of Figs. 4-15, we can see that mode 7 and 8 are weak. We cannot observe the modal patterns in the middle picture of Fig. 4-14. For the Korea Strait scenario, we can see weak modal pattern up to about 3 km range as shown in the upper picture of Fig. 4.14. The 8th mode shape in upper picture of Fig. 4.15 is weaker than the new 2nd layer scenario. The modal approach provides a simple and clear explanation of physics of scattering.

There is another approach to look at the scattered field using modes. A single mode excitation gives us easy and simple physical insights to know how the scattered field is affected

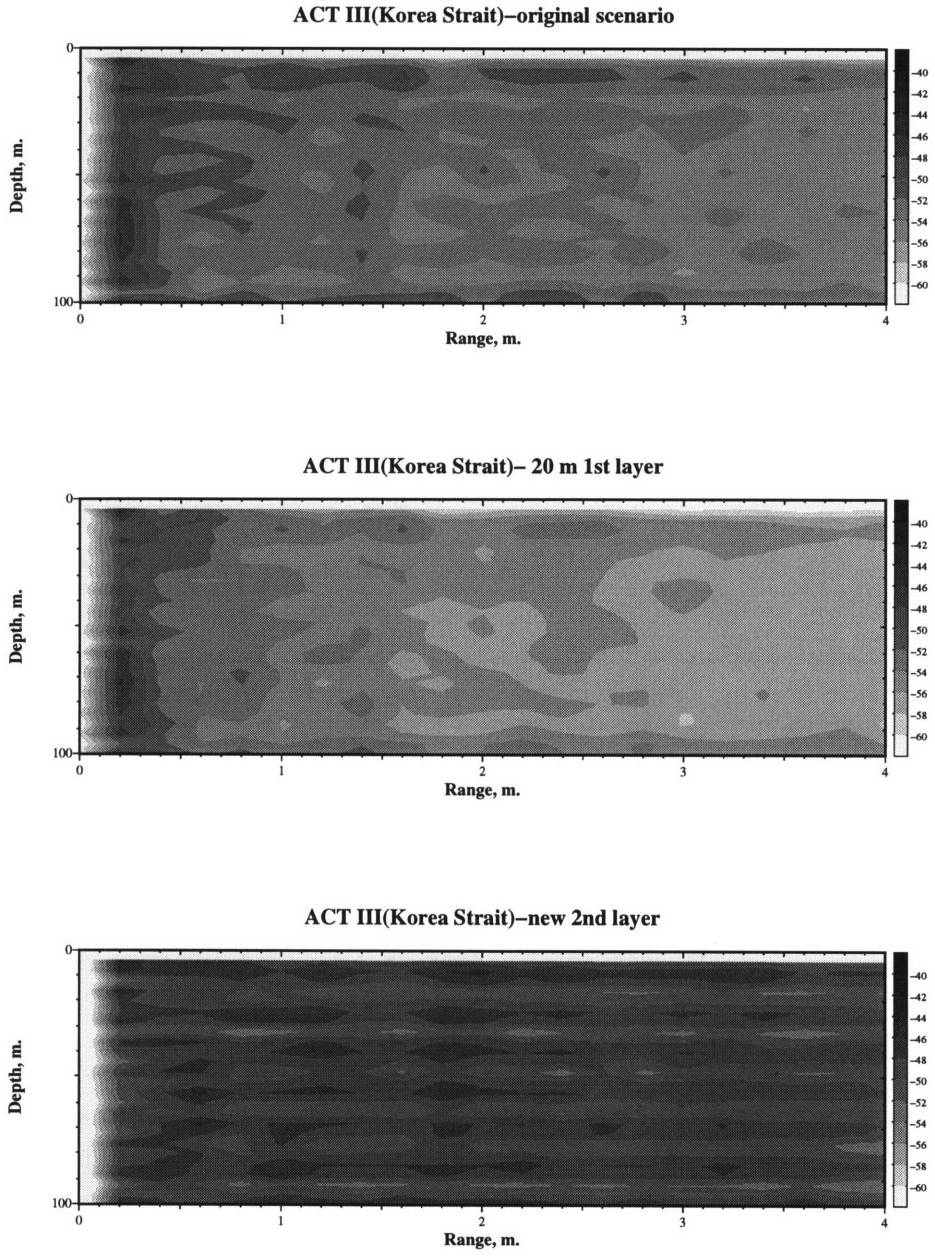

Figure 4-14: Scattered fields of three different scenarios. The upper picture is for the Korea Strait scenario, the middle one is for a 20 m 1st layer, and the last one is for a new 2nd layer.

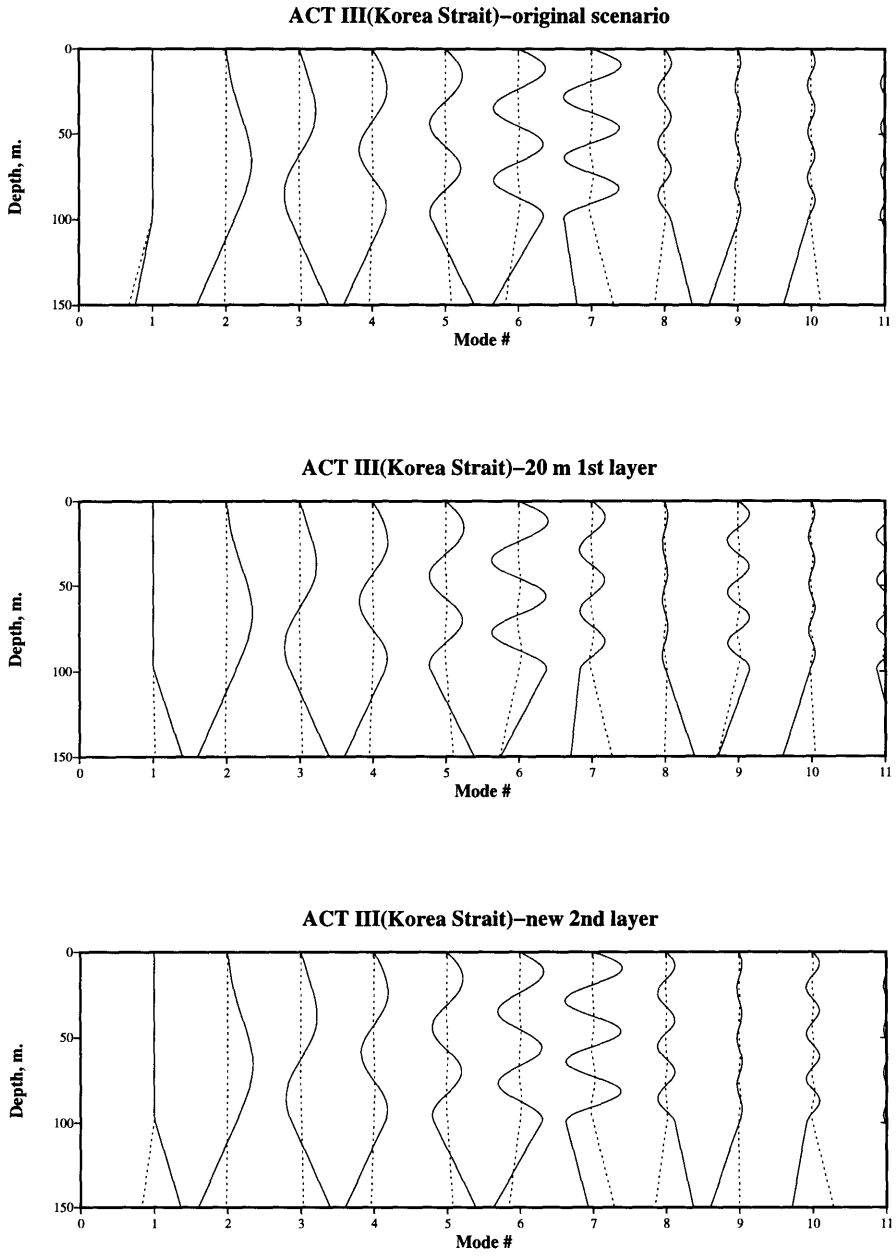

Figure 4-15: Mode shapes for the three scenarios. The upper picture is for the Korea Strait scenario, the middle one is for a 20 m 1st layer, and the last one is for a new 2nd layer.

by modes as stated in Chapter 3. Fig. 4-16 shows the scattered field modal amplitudes for excitation by modes 7,8 and 9 in the new 2nd layer scenario. All the proper modes excite the 8th mode strongly and the first leaky mode (9th mode) excites the 9th and 8th mode but they die out quickly. This results is consistent with the previous modal shape explanation. In this scenario the 8th mode is strongly excited by all proper modes and drives the scattered field.

We can also see similar phenomena in the Korea Strait scenario in Fig. 4-17. In this case, the 7th mode is excited strongly by the proper modes instead of the 8th mode. Compared with Fig. 4-16, the amplitude is small and dies quickly with range. The other adjacent modes are also excited although their amplitudes are smaller. That is the reason we cannot see strong modal patterns in the scattered field in Fig. 4-14. For 20 m 1st layer scenario, any particular mode is not excited strongly in Fig. 4-18. Instead all modes are excited and the amplitude is small compared with the two other scenarios as shown in Figs. 4-16 and 4-17. This also matches with the previous explanation.

The cross-modal coherence is another systematic way of looking at acoustic fields. The normalized total and forward-scattered fields are shown in Fig. 4-19. These pictures are from the original Korea Strait scenario. At 0.5 km range, the proper modes are not yet distinguishable in the total field so the coherence of all modes is high. In the scattered field, the modal coherence is not as high as in the mean field even at short ranges. At 4km range, the leaky modes become incoherent and only proper modes show high coherence in the total field. We can observe the 7th and 8th modes are relatively coherent with proper modes for the scattered field. At 50 km, only a few proper modes show some coherence for both the mean and scattered fields. All modes are totally incoherent, as evidenced by the fact that only diagonal terms are left. At this range the scattered fields become dominant in the total fields.

Although we tried to show the effects of the 1st layer thickness and the different type of the second layer on the scattered field, the scattered field is a more complex function of

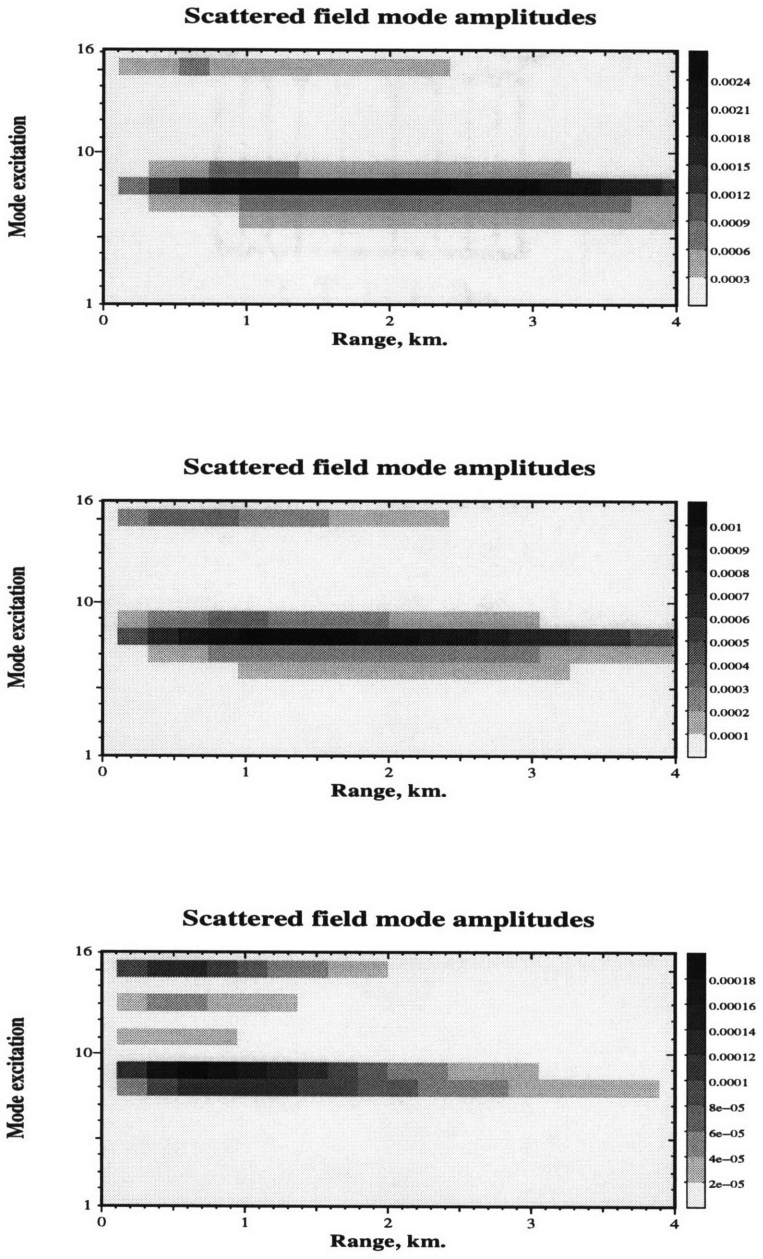

Figure 4-16: Scattered mode power for a single incident modes in the case of a new 2nd layer scenario. The top picture is for incident mode 7, the middle one is for incident mode 8, and the lower is for incident mode 9.

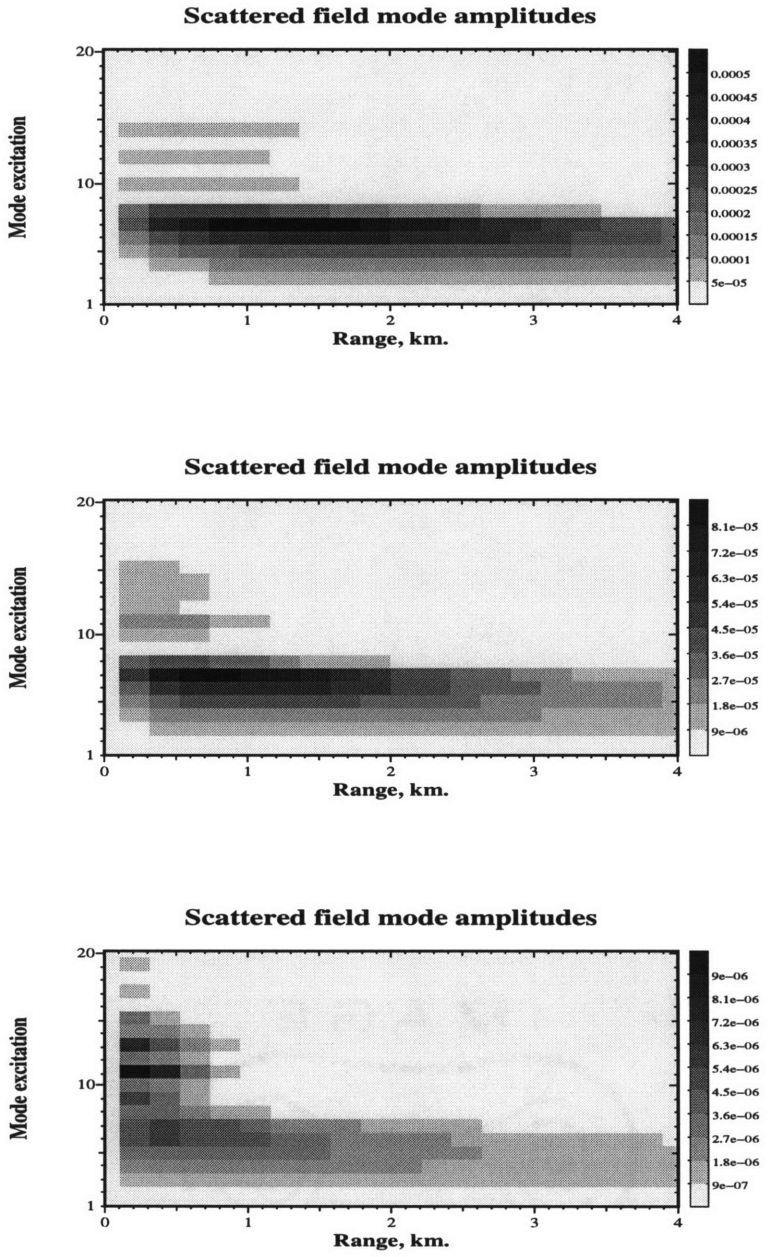

Figure 4-17: Scattered mode power for a single incident modes in the case of the Korea Strait scenario. The top picture is for incident mode 7, the middle one is for incident mode 8, and the lower is for incident mode 9.

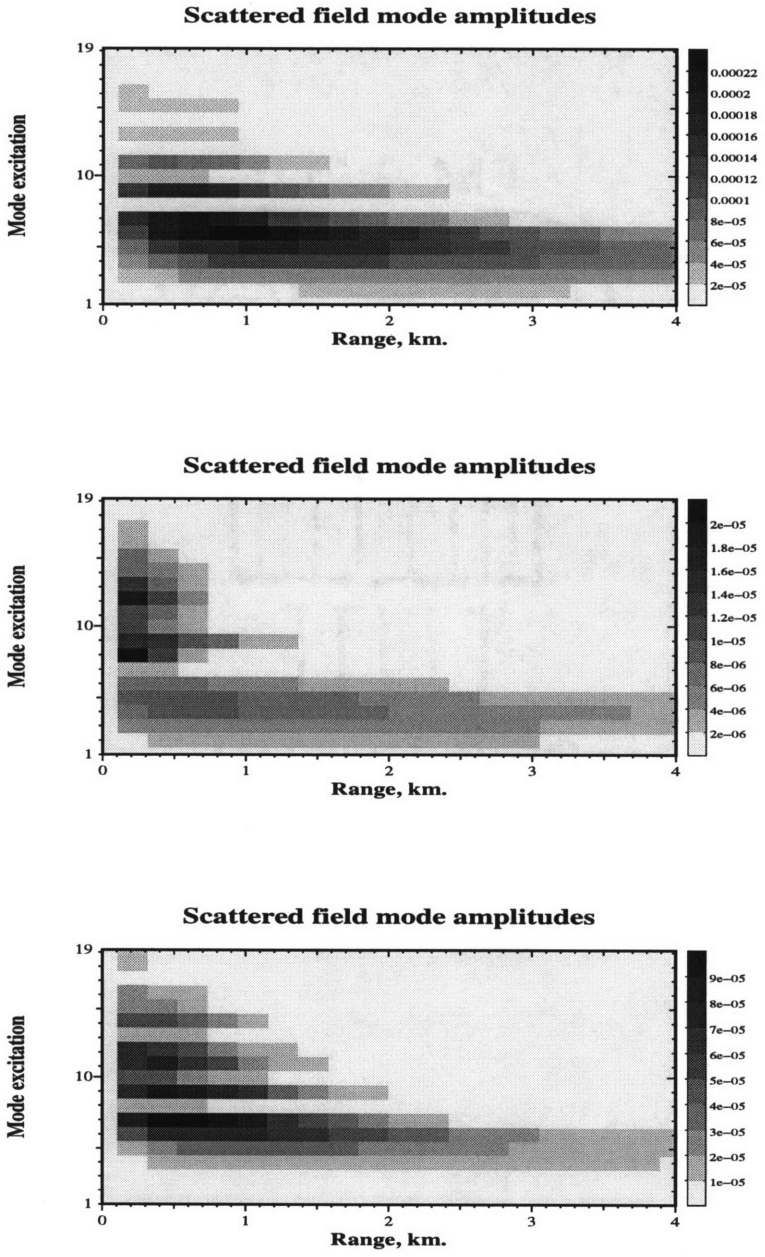

Figure 4-18: Scattered mode power for a single incident modes in the case of 20 m 1st layer scenario. The top picture is for incident mode 7, the middle one is for incident mode 8, and the lower is for incident mode 9.

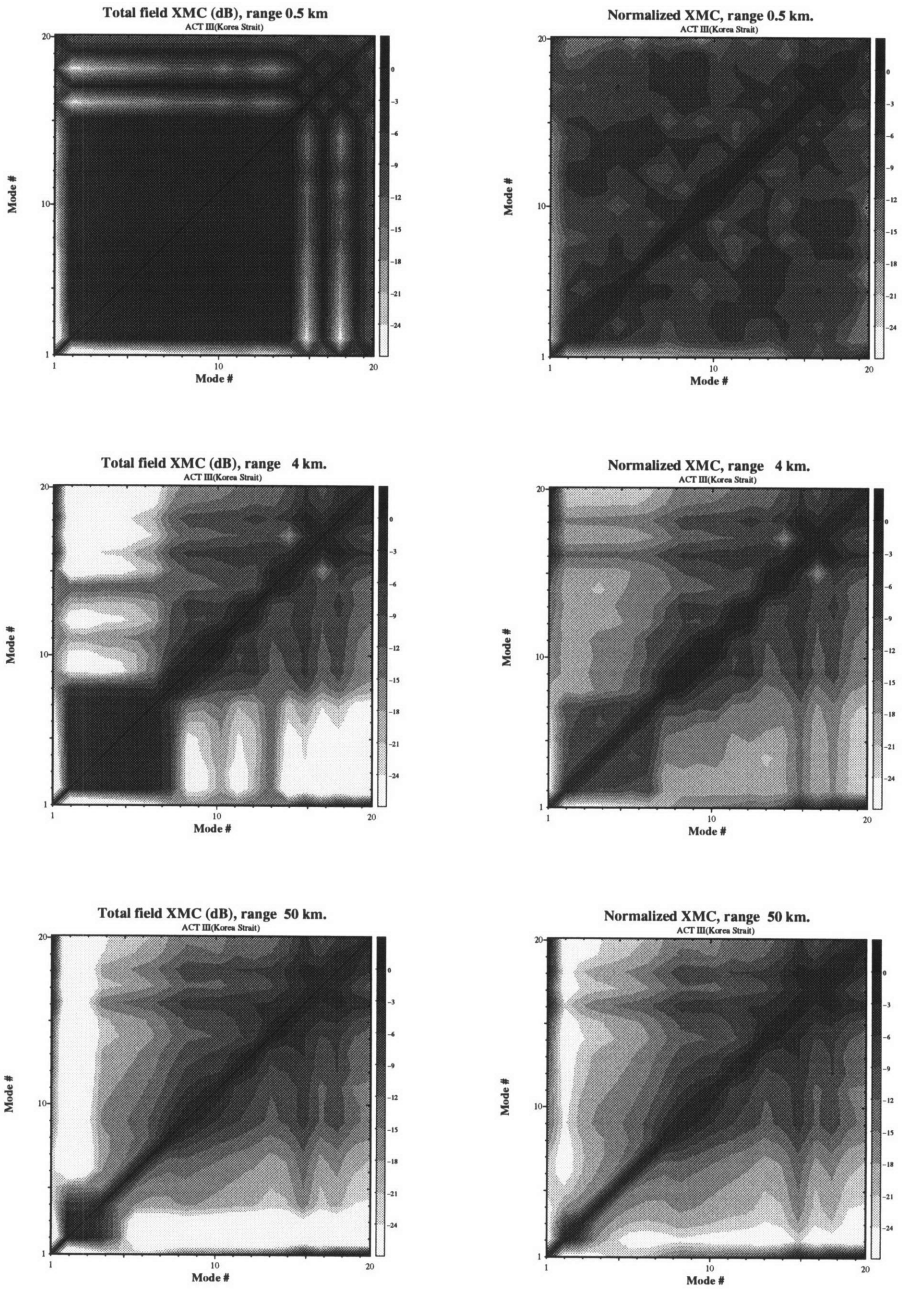

Figure 4-19: Cross-modal coherences(XMC) of the normalized total and scattered field for the Korea Strait Experiment scenario.

the sound speed profile in the water and the correlation length and RMS roughness heights, *etc.*. That means that the other parameters could affect the scattered field strongly and the thickness of the different bottom types might be hidden behind the more important parameters in some cases. We need to know the environmental parameters as precisely as possible. We also used many assumptions like range-independence, 2-dimensional scattering and neglect of multiple scattering from two or more rough surfaces *etc.*. However, we can conclude from these facts that the modal study of scattering is a good way to explain the scattered field and its mechanism.

4.3 Summary

We showed that extended version of NMSCAT can deal with arbitrary elastic layers to calculate the scattered field with some restrictions. These restrictions would be easily removed if a normal mode code were available to compute the mean fields in the elastic layers. The comparison with OASS results proved that NMSCAT can calculate the scattered field accurately in the case where the first or second elastic layer is thick enough or have strong attenuation.

We applied the extended NMSCAT to study the scattered field in the Korea Strait Experiment. Because the attenuation is quite high in the shelly silty sand layer which has 10 m thickness below the water column, we can use NMSCAT to model the experiment and the results show a quite good agreement with ones from OASS.

We can easily see the differences in the scattered field when the thickness of the first layer is changed from 10 m to 20 m. The properties(density, the sound speeds) of the second layer also affect the scattered field significantly. The scattered field is driven by the 8th mode because this mode is resonant in the elastic layer. The modal approach gives good and easy explanations of these scattering phenomena.

This means that the scattered field is proven to be a good way to study the thickness of the elastic layer. If we study the mean fields and the scattered fields together, it will provide

more information about the thickness of the first elastic layer. We propose as further study to extract the thickness of the first elastic layer from the scattered and mean fields by an inverse method.

Chapter 5

Conclusion and Future Study

5.1 Conclusion

The main contribution of this thesis is to develop the extended version of the normal mode scattering code NMSCAT and to use this code to study scattering considering the elastic layers in the waveguide. This code can deal with any arbitrary elastic layers to calculate the scattered field with some restrictions. The scattered fields computed by NMSCAT are in good agreement with the ones by our benchmark, OASS, except at short range. The error is within 2 dB when we consider one limestone layer over a half basalt space. The restrictions on the validating regions come from errors in the calculation of the mean fields in the elastic layers using the normal mode code KRAKENC. This restriction could be removed easily if a normal mode code like ORCA is used to compute the displacement and stress of the mean fields in the elastic layers. Although NMSCAT has these restrictions currently, it is still a good way to study scattered fields if we model the first two elastic layers as thick or having high attenuation. In these cases, the error is quite small when we compare the results with OASS. The Korea Experimental geoacoustic data is used to simulate the scattered field. The bottom in the Korea Strait is composed of 3 elastic layers including a moraine half space. We studied the effects of the thickness of the 1st layer and the different bottom properties

in the 2nd layer on the scattered field. Their effects are quite distinct and are analyzed by the modal approach.

The modal approach to study the scattered fields is shown to have some advantages. One is the computational efficiency at the long ranges as compared with OASS, which is the wave number integral method. Although the computational efficiency of normal mode scattering is not the focus of this thesis (see reference [40]), efficient computation is very important in studying the scattering because scattering requires heavy computation.

Another merit of modal scattering is the intuitive understanding of the underlying physics that it can provide. The mode shapes keep interpret the physics of scattering as do single mode excitations and cross-modal coherences. Moreover, the modal analysis may provide good hints to plan the acoustic experiments to study the bottom properties by prescribed modal excitation and cross-modal analysis.

The scattered fields are strongly affected by thickness and the properties of elastic layers. We can infer from these facts that the scattered fields may provide a good way to study the bottom properties such as thickness and the sound speed of the layer. This is because the scattered fields are driven by both the mean fields themselves, and the derivative of the mean fields at the rough interface with the discontinuities of the scattered field and its derivative at the rough surface. The scattered field is usually more sensitive to thickness, sound speeds, number of layers or other properties than the mean field. The pattern of change of the scattered fields as a function of these parameters do not agree with the one in the mean fields. Therefore, if we study the bottom properties by the scattered fields and the mean fields together, we can get more information about the bottom.

5.2 Future Study

The extended NMSCAT is an integrated modal code to calculate the scattered field in the waveguide considering arbitrary elastic layers. Although it is a versatile tool to study the statistical scattering, it involves some assumptions and restrictions.

First, we have to calculate the displacement and stress vectors of the mean field by modes in the elastic layers in order to get rid of the restraints discussed in Chapter 2 and 4. Then we can compute the scattered field in the water column accurately for arbitrary layers without any restrictions. We can also deal with any rough surface in the elastic layers. The scattered fields in the all elastic layers could also be calculated if we obtain each up- and down-going wave components. Then a versatile and applicable modal code could be completed. The integrated modal code will be very helpful to study the scattering mechanism and physics.

One of the advantages of a modal approach is the easy extension to other environments like range-dependent and 3 dimensional environments. Shallow water is highly range dependent because of the bottom topography and the inhomogeneities in the water itself in the form of wave fronts, solitons and solibores with strong currents and tides. The normal mode code for the mean field propagation can incorporate these complex environments so the modal scattering code might also involve these complex environments although more research is necessary. For the shallow water waveguide, the range dependence would often be important. Scattering might be affected significantly by the range dependence. Then the scattering theory could be modified in the same way as adiabatic or coupled mode theory for the mean field. For high frequency scattering at short ranges, the 3 dimensional scattering could be important for accurate calculation of the scattered field. Although the initial approach was suggested by Tracey with cylindrical coordinates, a further study should be focused on non-symmetric environments for full 3 dimensional scattering.

We suggested that the bottom properties might be studied by scattering with mean field in the shallow water waveguide. We just showed that the scattered field is affected strongly by the bottom properties, such as thickness, bottom properties and number of layers. We can infer from this fact carefully that the bottom properties might be extracted by the scattering signals using inverse methods. Forward problems should be studied first with many parameter studies. The scattering prediction is more dependent on the environment than the mean field prediction. Therefore the consideration of many parameters is absolutely necessary for prediction.

Finally, experimental data should be compared with the scattered field calculated by numerical models using measured environmental parameters. Although many unknown effects of some parameters and their effect on scattering are not well understood yet, intelligent approximations, restrictions and careful selection of the most important parameters should make it possible to compute the expected scattered field and compare it favorably with the experimental data. Then we can understand the mechanisms and the physics of scattering more clearly.

Appendix A

Realization of the Rough Surfaces

A.1 Realization of the Rough Surfaces

When we describe the rough surface in the stochastic theory, two main functions are required to represent roughness in the 1 dimensional rough surface. One is the correlation function and the other is the RMS height function. The power spectrum of the rough surface is usually used on this purpose.

The Goff-Jordan[17] showed that the power law spectra can represent the real rough bottom better than the Gaussian spectra because the power law can use different scales and include higher frequency terms. The Gaussian spectra have some advantages to incorporate its formula with other mathematics in a simple way so it is still valid and useful in some problems.

The Gaussian spectrum and the Goff-Jordan spectrum used in this paper are expressed by,

$$P(k) = \sqrt{2\pi}Le^{-(kL)^2} \tag{A.1}$$

$$P(k) = \pi L[(kL)^2 + 1]^{-1.5} \tag{A.2}$$

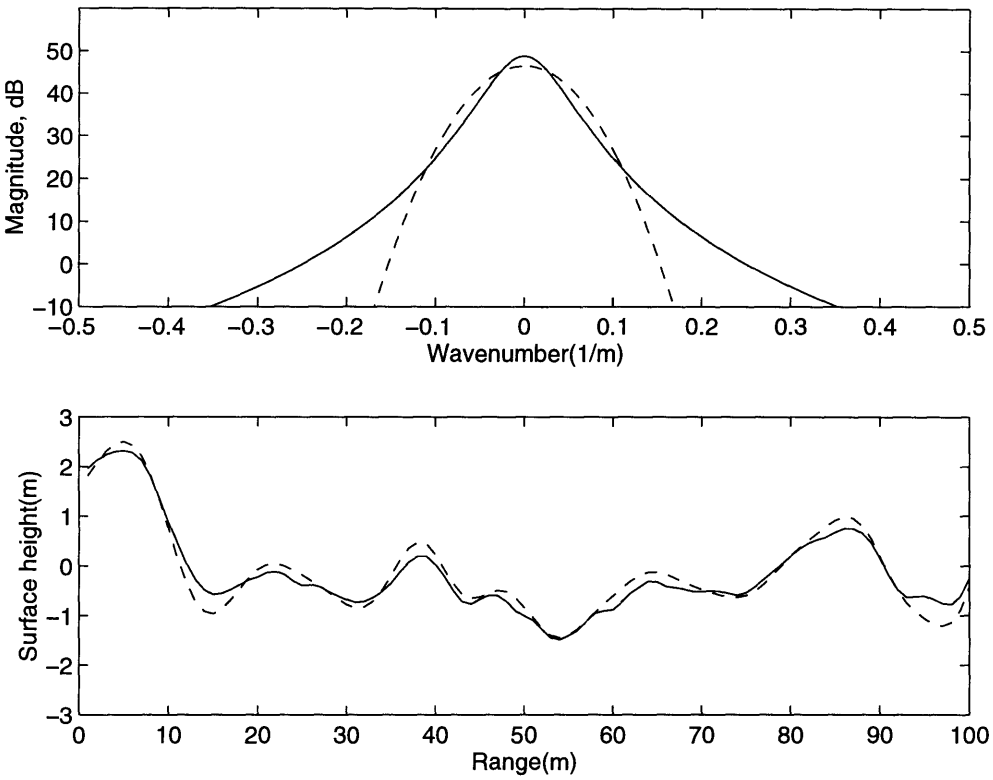

Figure A-1: Realization of the rough surfaces for two types of spectra. Solid line is for the Goff-Jordan power spectrum and the dashed line is for the Gaussian spectrum.

where L is the correlation length k is the wave number.

As Fig. A-1 shows two spectra, the Goff-Jordan spectrum includes high energy in the high wavenumbers. One of the realizations from two power spectra is shown in this figure, too. The RMS height is 1 m in the realization. As we can expect, the higher order oscillation are observed in the realization of the rough surface from the Goff-Jordan spectrum. The effects of the higher order on the scattered field were mentioned in Tracey's thesis[40].

Bibliography

[1] G.V. Anand and M.K. George. Normal mode sound propagation in an ocean with random narrow-band waves. *J. Acoust. Soc. Am.*, 94(1):279–292, July 1993.

[2] F.G. Bass and I.M. Fuks. *Wave scattered from statistically rough surfaces.* Pergamon, Oxford, 1979.

[3] E.O. Bautista and R.D. Stoll. Remote determination of *in situ* sediment parameters using love waves. *J. Acoust. Soc. Am.*, 98(2):1090–1096, August 1995.

[4] A.T. Bharucha-Reid. *Probabilistic methods in applied mathematics.* Academic Press, New York, 1968.

[5] L.M. Brekhovskikh. *Waves in layered media.* Academic Press, New York and London, second edition, 1980.

[6] L.M. Brekhovskikh and Yu.P. Lysanov. *Fundamentals of Ocean Acoustics.* Springer-Verlag Berlin Heidelberg, New York, 1982.

[7] J.R. Buck, J.C. Preisig, J. Johnson, and J. Catipovic. Single-mode excitation in the shallow-water acoustic channel using feedback control. *IEEE Journal of Ocean Engineering*, 22(2):281–291, April 1997.

[8] H.P. Bucker and H.E. Morris. Normal-mode reverberation in channels or ducts. *J. Acoust. Soc. Am.*, 44:827–828, 1968.

[9] A. Caiti and S.M. Jesus. Acoustic estimation of seafloor parameters:a radial basis functions approach. *J. Acoust. Soc. Am.*, 100(3):1473–1481, September 1996.

[10] D.D. Ellis. Shallow-water reverberation:normal-mode model predictions compared with bistatic towed-array measurements. *IEEE Journal of Ocean Engineering*, 18:474–482, 1993.

[11] D.D. Ellis. A shallow-water normal-mode reverberation model. *J. Acoust. Soc. Am.*, 97(5):2804–2814, May 1995.

[12] D.D. Ellis and D.V. Crowe. Bistatic reverberation calculations using a three-dimensional scattering function. *J. Acoust. Soc. Am.*, 89(5):2207–2214, May 1991.

[13] H.H. Essen. Scattering from a rough sedimental seafloor containing shear and layering. *J. Acoust. Soc. Am.*, 95(3):1299–1310, March 1994.

[14] P.C. Etter. *Underwater Sound Acoustic Modeling-Principles, Techniques and Applications.* Elsevier Applied Science, London and New York, second edition, 1996.

[15] E.R. Franchi, J.M. Griffin, and B.J. King. Nrl reverberation model:a computer program for the prediction and analysis of medium- to long-range boundary reverberation. Report 8721, Naval Research Laboratory, Washington DC, 1984.

[16] G.V. Frisk. *Ocean and Seabed Acoustics.* Prentice-Hall, Berlin, Heidelberg, New York, first edition, 1993.

[17] J.A. Goff and T.H. Jordan. Stochastic modeling of seafloor morphology: Inversion of sea beam data for second order statistics. *J. Geophys. Res.*, 93:13589–13608, 1993.

[18] A. Ishimaru. *Wave propagation and scattering in random media.* Academic Press, New York, 1978.

[19] F.B. Jensen, W.A. Kuperman, M.B. Porter, and H.Schmidt. *Computational Ocean Acoustics.* American Institute of Physics, Woodbury, New York, 1994.

[20] V.M. Kudryashov. Influence of shear elasticity on the scattering of sound by a plate with statistically rough boundaries. *Sov. Phys. Acoust.*, 33(6):625–627, Nov.-Dec. 1988.

[21] W.A. Kuperman and F. Ingenito. Attenuation of the coherent component of sound propagation in shallow water with rough boundaries. *J. Acoust. Soc. Am.*, 61:1178–1187, 1977.

[22] W.A. Kuperman and H. Schmidt. Rough surface elastic wave scattering in a horizontally stratified ocean. *J. Acoust. Soc. Am.*, 79:1767–1777, 1986.

[23] W.A. Kuperman and H. Schmidt. Self-consistent perturbation approach to rough surface scattering in stratified elastic media. *J. Acoust. Soc. Am.*, 86(4):1511–1522, October 1989.

[24] J.F. Lynch, P. Bucca, A.E. Newhall L. Fu, S.D. Rajan, and J. Fulford. The effect of fronts and internal waves on acoustic propagation prediction for the act iii exercise in the strati of korea. *IEEE Journal of Ocean Engineering*, submitted in 1997.

[25] H. Matsumoto, R.P. Dziak, and C.G. Fox. Estimation of seafloor microtopographic roughness through modeling of acoustic backscatter data recorded by multibean sonar systems. *J. Acoust. Soc. Am.*, 94:2776–2787, 1993.

[26] J.A. Ogilvy. Wave scattering from rough surfaces. *Rep. Prog. in Physics*, 50:1553–1608, 1987.

[27] C.L. Pekeris. Theory of propagation of explosive sound in shallow water. *Geol. Soc. Am. Mem.*, 27, 1948.

[28] D. Peregrym. An inverstigation of shallow water mode coupling effects during single mode transmission. Master's project, MIT/WHOI Joint Program Oceanography and Oceanographic Engineering, Woods Hole, MA, August 1994.

[29] M.B. Porter. The kraken normal mode program. Technical report, 1992.

[30] D. Rouseff and T. Ewart. Effect of random sea surface and bottom roughness on propagation in shallow water. *J. Acoust. Soc. Am.*, 98(6):3397–3404, December 1995.

[31] H. Schmidt. Oases: Seismo-acoustic fast field algorithm for range independent environments, user's guide. Technical report, 1997.

[32] H. Schmidt and F.B. Jensen. An efficient numerical solution technique for wave propagation in horizontally stratified environments. *Comp. Math. Appl.*, 11:699–716, 1985.

[33] H. Schmidt and W.A. Kuperman. Spectral representations of rough interface reverberation in stratified ocean wavequide. *J. Acoust. Soc. Am.*, 97(4):2199–2209, October 1995.

[34] H.G. Schneider. Moccasin:sound propagation and sonar range prediction model for shallow water environments. TB 1990-9, FWG, Kiel, Germany, 1990.

[35] E.C. Shang. Some new challenges in shallow water acoustics. In H.M. Merklinger, editor, *Progress in Underwater Acoustics.* Plenum, New York, 1987.

[36] K.B. Smith and W.S. Hodgkiss. Propagation and analysis issues in the prediction of long-range. *J. Acoust. Soc. Am.*, 99(3):1387–1404, March 1996.

[37] R.A. Stephen and S.A. Swift. Modeling seafloor geoacoustic interaction with a numerical scattering chamber. *J. Acoust. Soc. Am.*, 96(2):973–990, August 1994.

[38] R.D. Stoll and E.O. Bautista. New tools for studying seafloor geotechnical and geoacoustic properties. *J. Acoust. Soc. Am.*, 96(5):2937–2944, November 1994.

[39] R.D. Stoll, G.M. Bryan, and E.O. Bautista. Measuring lateral variability of sediment geoacoustic properties. *J. Acoust. Soc. Am.*, 96(1):427–438, May 1994.

[40] B.H. Tracey. *An integrated modal approach to surface and volume scattering in ocean acoustic waveguides.* PhD thesis, Massachusetts Institute of Technology and Woods Hole Oceanographic Institution, January 1995.

[41] B.H. Tracey and H. Schmidt. Seismo-acoustic field statistics in shallow water. *IEEE Journal of Ocean Engineering*, 100(2):317–331, April 1997.

[42] H. Weingberg. The generic sinar model. Technical Document 5971D, Naval Underwater Systems Center, New London, 1985.

[43] E.K. Westwood, C.T. Tindle, and N.R. Chapman. A normal mode model for acousto-elastic ocean environments. *J. Acoust. Soc. Am.*, 100(6):3631–3645, December 1996.

[44] A. Wirgin. Reflection from a corrugated surface. *J. Acoust. Soc. Am.*, 68:692–699, 1980.

[45] R. Zhang and G. Jin. Normal-mode theory of average reverberation intensity in shallow water r. *J. Sound and Vibration*, 119(2):215–223, 1987.

[46] J. Zhou, X. Zhang, and P. Rogers. Resonant interaction of sound wave with internal solitons in the coastal zone. *J. Acoust. Soc. Am.*, 90:2042–2854, 1991.